

# CEBAF Program Advisory Committee Six (PAC6) Proposal Cover Sheet

This proposal must be received by close of business on April 5, 1993 at:

CEBAF  
User Liaison Office  
12000 Jefferson Avenue  
Newport News, VA 23606

## Proposal Title

Measurement of the Deuteron Tensor Polarisation at Large Momentum Transfers  
in  $D(e, e' \vec{d})$  Scattering

## Contact Person

**Name:** KOX Serge  
**Institution:** Institut des Sciences Nucléaires  
**Address:** 53, Av. des Martyrs  
**Address:** 38026 - GRENOBLE-CEDEX (France)  
**City, State ZIP/Country:**  
**Phone:** 76.28.41.55      **FAX:** 76.28.40.04  
**E-Mail → BITnet:** KOX @ FRCPN11      **Internet:**

**If this proposal is based on a previously submitted proposal or  
letter-of-intent, give the number, title and date:**

Partly based on the letter of Intent LOI 61  
High Momentum Transfer Measurement of the Recoil Deuteron Tensor Polarization  
in Elastic Electron Deuteron Scattering  
10/1/1987

## CEBAF Use Only

Receipt Date: 4/1/93      Log Number Assigned: PR 93-003

By: SA

Measurement of the Deuteron Tensor  
Polarization at Large Momentum Transfers in  
 $D(e, e' \vec{d})$  Scattering.

J. Arvieux <sup>a</sup>, G. Audit <sup>b</sup>, Th.S. Bauer <sup>c</sup>, E.J. Beise <sup>d</sup>, L. Bimbot <sup>e</sup>, E. Brash <sup>f</sup>, J.M. Cameron <sup>g</sup>,  
C.C. Chang <sup>d</sup>, J.E. Ducret <sup>b</sup>, G.W. Dodson <sup>h</sup>, K. Dow <sup>h</sup>, M. Farkhondeh <sup>h</sup>, B. Frois <sup>b</sup>,  
C. Furget <sup>i</sup>, M. Garçon <sup>b</sup>, R. Gilman <sup>f</sup>, C. Glashauser <sup>f</sup>, S. Høibråten <sup>j\*</sup>, J. Jourdan <sup>k</sup>,  
S. Kox <sup>i</sup>, B. Ni <sup>g</sup>, S. Platchkov <sup>b</sup>, R. Ransome <sup>f</sup>, J.S. Real <sup>i</sup>, P. Roos <sup>d</sup>, P. Rutt <sup>f</sup>,  
E.J. Stephenson <sup>g</sup>, E. Tomasi-Gustafsson <sup>a\*</sup>, W. Turchinets <sup>h</sup>, E. Voutier <sup>i</sup>.

<sup>a</sup> Laboratoire National Saturne, IN2P3-CNRS and DSM-CEA,  
F-91191 Gif-sur-Yvette, France.

<sup>b</sup> DAPNIA/Service de Physique Nucléaire, CEN Saclay,  
F-91191 Gif-sur-Yvette, France.

<sup>c</sup> University of Utrecht, P.O. Box 80.000, 3508 TA Utrecht, The Netherlands.

<sup>d</sup> University of Maryland, College Park, Maryland 20742, USA.

<sup>e</sup> Institut de Physique Nucléaire, F-91400 Orsay, France.

<sup>f</sup> Rutgers University, Box 849, Piscataway, N.J. 08854, USA.

<sup>g</sup> IUCF, Bloomington, Indiana 47405, USA.

<sup>h</sup> MIT/Bates, Cambridge, Massachusetts, 02139, USA.

<sup>i</sup> Institut des Sciences Nucléaires, IN2P3-UJF, F-38026 Grenoble Cedex, France.

<sup>j</sup> University of Virginia, Charlottesville, USA.

<sup>k</sup> Institut fuer Physik, CH-4056 Basel, Switzerland.

\* To be confirmed.

S. Kox <sup>i</sup> (Spokesperson) and E.J. Beise <sup>d</sup> (Co-spokesperson)

(List of collaborators not yet finalized)

## ABSTRACT

We propose to extend the existing measurements of the tensor polarization of the deuteron produced in the  $D(e, e' d)$  elastic scattering. Using the CEBAF facility and a new deuteron tensor polarimeter (*POLDER*), the  $t_{20}$  of the recoiling deuteron will be measured in the range of momentum transfer  $Q = 4.4 - 6.2 \text{ fm}^{-1}$ . When combined with the knowledge of the structure functions  $A$  and  $B$ , this quantity permits the separation of the charge ( $G_C$ ) and quadrupole ( $G_Q$ ) form factors of the deuteron. The determination of  $G_C$  at large momentum transfer will test the applicability of existing theoretical models and their assumptions, and determine the effects of non-nucleonic degrees of freedom.

---

April 2, 1993

# 1 Introduction

The deuteron has a spin 1 and its electromagnetic structure is described by three form factors: charge monopole  $G_C$ , charge quadrupole  $G_Q$  and magnetic dipole  $G_M$ . Non-relativistically, these form factors are related to the spatial distributions of charge, quadrupole deformation and magnetization respectively, both the nucleon spins and the nucleon currents contributing to the latter.

Many models of the deuteron electromagnetic form factors have been proposed. In the impulse approximation (IA) for the description of  $e$ - $d$  scattering, the electron interacts with each nucleon in the deuteron via a virtual photon and the electromagnetic form factors of the interacting nucleon are taken to be the same as those for a free nucleon. At large four-momentum transfers, various corrections to the IA become important. These include isoscalar meson-exchange currents (MEC), isobar components (IC), relativistic effects and perhaps quark degrees of freedom. Relativistic models have been developed in both the light cone formalism and solving a Bethe-Salpeter equation. Some non-relativistic models use a coupled-channel formalism of nucleons and isobars ( $\Delta$  and  $N^*$ ) and include contributions from MEC; in these models the amount of  $\Delta$ - $\Delta$  component in the deuteron ranges from 0.4 to 7 %. Quark configurations are incorporated in several hybrid quark-hadron models with the quark confinement radius taken as a free parameter. Some of these models give predictions similar to the IA while others have completely different results for the high four-momentum transfer region. A Skyrme model predicts results for the deuteron form factors similar to those obtained from conventional nucleon-meson dynamics. Finally, perturbative quantum chromodynamics (PQCD) predicts simple relations between the form factors of the deuteron.

Experimentally, at least three observables of  $e$ - $d$  scattering are needed to determine separately all three form factors (see section 2). Differential cross-sections measurements at different electron angles for the same four-momentum transfer allow the determination of the longitudinal and transverse structure functions  $A(G_C^2, G_Q^2, G_M^2)$  and  $B(G_M^2)$ , which have been so far the main testing ground for the above mentioned models.  $A$  is measured up to  $Q = 10 \text{ fm}^{-1}$  [1] and  $B$  up to  $Q = 8 \text{ fm}^{-1}$  [2]. To separate further  $G_C$  and  $G_Q$ , the measurement of another observable is required, and this is necessarily a polarization observable. This fact was realized a long time ago : one must either measure the asymmetries induced by a tensor polarized deuterium target, or measure the tensor polarization of the recoiling deuterons (alternatively, one may deal with deuteron vector polarization only if the electron beam is polar-

ized; this type of experiment has never been attempted, but is not expected to yield a better determination of the individual form factors [3]). The observable of choice here is the tensor moment  $t_{20}$  which is a measure of the relative probabilities of scattering off deuterons in magnetic substates  $m_z = +1, -1$  or  $0$  when dealing with a polarized target, or of producing deuterons in these different magnetic substates when measuring the polarization of the outgoing deuterons.  $t_{20}(G_C, G_Q, G_M, \theta_e)$ , together with  $A(G_C^2, G_Q^2, G_M^2)$  and  $B(G_M^2)$ , allows the separate determination of the two charge form factors  $G_C$  and  $G_Q$ . The two other tensor moments  $t_{21}$  and  $t_{22}$  provide also different useful quadratic combinations of the form factors.

Some measurements of  $t_{20}$  [4, 5, 6, 7, 8] have been performed at relatively low momentum transfer where theoretical uncertainties are very small and predictions differ only little from each others. The recent Bates experiment, performed with the polarimeter AHEAD [9], determined all three moments of the recoiling deuterons tensor polarization ( $t_{20}$ ,  $t_{21}$  and  $t_{22}$ ) at four-momentum transfer values up to  $Q = 4.62 \text{ fm}^{-1}$  [10], and provided the first experimental evidence for a node in  $G_C$  (located around  $4.4 \text{ fm}^{-1}$ ). This node is a reflection of a node in the S-state wave function, which in turn is due to the repulsive nature of the NN interaction at short distances. Thus around  $4\text{-}5 \text{ fm}^{-1}$ , the already measured structure function  $A$  determines mostly  $G_Q$ . At such four-momentum transfers, short-range components and non-nucleonic contributions become important and manifest themselves mainly in  $G_C$ . Finally, contrary to all other observables and to the form factors themselves,  $t_{20}$  is nearly independent of the elementary nucleon form factors, and in particular of the poorly known neutron electric form factor.

We are proposing here to perform new precise measurements of  $t_{20}$ ,  $t_{21}$ , and  $t_{22}$ , starting at  $4.4 \text{ fm}^{-1}$  to determine with better accuracy the behaviour of  $G_C$  around its node and extending the separate determination of  $G_C$  and  $G_Q$  up to  $6.2 \text{ fm}^{-1}$ .

## 2 Kinematics and observables

The energies of the incident ( $E_e$ ) and scattered ( $E'_e$ ) electrons, and of the deuteron ( $T_d$ ) are related to  $Q$  by the relation :

$$Q^2 = 2 M_d T_d = 2 M_d (E_e - E'_e) = 4 E_e E'_e \sin^2 \left( \frac{\theta_e}{2} \right) \quad (2.1)$$

where  $M_d$  is the deuteron mass and  $\theta_e$  the scattering angle of the electron.

It is also convenient to express the angular correlation as :

$$\sin^2(\theta_d) = \frac{\cos^2\left(\frac{\theta_e}{2}\right)}{1 + \mu \sin^2\left(\frac{\theta_e}{2}\right)} \iff \sin^2\left(\frac{\theta_e}{2}\right) = \frac{\cos^2(\theta_d)}{1 + \mu \sin^2(\theta_d)} \quad (2.2)$$

with

$$\mu = \left( \frac{E_e}{M_d} \right)^2 + \frac{2E_e}{M_d} \quad (2.3)$$

By using the first Born approximation (one-photon exchange approximation) and imposing relativistic and gauge invariance, the differential cross-section can be written as

$$\frac{d\sigma}{d\Omega} = \left( \frac{d\sigma}{d\Omega} \right)_{Mott} \cdot S \quad (2.4)$$

where

$$\left( \frac{d\sigma}{d\Omega} \right)_{Mott} = \frac{\alpha^2 E'_e \cos^2\left(\frac{\theta_e}{2}\right)}{4 E_e^3 \sin^4\left(\frac{\theta_e}{2}\right)} \quad (2.5)$$

describes the scattering of an electron off a pointlike spinless particle ( $\alpha$  is the fine structure constant), and

$$S = A(Q) + B(Q) \tan^2 \left( \frac{\theta_e}{2} \right) \quad (2.6)$$

originates from the electromagnetic structure of the deuteron. As a consequence of parity and time-reversal invariance, the structure functions  $A$  and  $B$  are in turn given in terms of three elementary electromagnetic form factors:

$$A(Q) = G_C^2(Q) + \frac{8}{9} \eta^2 G_Q^2(Q) + \frac{2}{3} \eta G_M^2(Q) \quad (2.7)$$

$$B(Q) = \frac{4}{3} \eta (1 + \eta) G_M^2(Q) \quad (2.8)$$

with  $\eta = Q^2/4M_d^2$ .

The three moments  $t_{2q}$  of the deuteron tensor polarization are given by:

$$t_{20} = -\frac{1}{\sqrt{2} S} \left[ \frac{8}{3} \eta G_C G_Q + \frac{8}{9} \eta^2 G_Q^2 + \frac{1}{3} \eta [1 + 2(1 + \eta) \tan^2 \left( \frac{\theta_e}{2} \right)] G_M^2 \right] \quad (2.9)$$

$$t_{21} = \frac{2}{\sqrt{3} S} \eta [\eta + \eta^2 \sin^2 \left( \frac{\theta_e}{2} \right)]^{1/2} G_M G_Q \sec \left( \frac{\theta_e}{2} \right) \quad (2.10)$$

$$t_{22} = -\frac{1}{2\sqrt{3} S} \eta G_M^2 \quad (2.11)$$

In the one photon-exchange approximation of  $e$ - $d$  scattering, and as a result of time-reversal invariance, the deuteron vector polarization is identically zero when using an unpolarized electron beam.

The form factors are normalized at  $Q = 0$  to the static moments:

$$G_C(0) = 1 \quad (2.12)$$

$$G_Q(0) = M_d^2 Q_d = 25.83 \quad (2.13)$$

$$G_M(0) = \frac{M_d}{M_p} \mu_d = 1.714. \quad (2.14)$$

where  $Q_d$  and  $\mu_d$  are respectively the electric quadrupole moment and the magnetic dipole moment of the deuteron, and  $M_p$  is the proton mass.

The quantity  $\bar{t}_{20}$  derived from Eq. 2.9 by neglecting the magnetic contribution is often used in the literature. Though not an observable, it is interesting since it depends solely on the ratio

$$x = \frac{2}{3} \eta G_Q / G_C \quad (2.15)$$

$$\bar{t}_{20} = -\sqrt{2} \frac{x(x+2)}{1+2x^2} \quad (2.16)$$

At small four-momentum transfers,  $x \ll 1$  and  $t_{20} \simeq \bar{t}_{20} \simeq -2x\sqrt{2} \simeq -\frac{\sqrt{2}}{3} Q_d Q^2$ , so that  $t_{20}$  is very much constrained by the already known deuteron quadrupole moment. The maximum difference between  $\bar{t}_{20}$  and  $t_{20}$  occurs around their absolute minimum (i.e. when  $x=1$ ) and is of the order of 10-15%.

### 3 The Physics Case

In this section we review some of the existing theoretical calculations of the deuteron form factors and compare available data with these model predictions. However, for sake of clarity we will present only one figure (figure 1) with a sample of representative calculations discussed below which are compared with existing experimental data.

#### 3.1 Nonrelativistic impulse approximation

In the NRIA,  $G_C(Q)$  has a structure very similar to  $u(k)$ , the S-state wave function in momentum space, with  $k$ , the momentum of the nucleons with respect to their center of mass, equal to  $Q/2$  [11]. The weaker the short-range repulsion of the NN potential, the more the node of  $u(k)$  will move to higher values, the shallower the minimum of  $G_C$  and the less steep the slope of  $t_{20}$  will appear. At the limit where the hard core disappears, the node moves to infinity and  $\bar{t}_{20}$  remains lower than  $-1/\sqrt{2}$ . NN potentials developed in the last ten years all incorporate the main features of the NN scattering data. But phase-shift equivalence does not imply equal potential or wave-function, and therefore differences may manifest themselves in the deuteron form factors. In the case of the Bonn potential (Bonn-E) [12], the calculation must take care of its explicit energy dependence [13]. Calculations of the deuteron form factors and  $e-d$  observables in the NRIA have been performed by many authors [12, 14, 15, 16, 17, 18]. It is remarkable that the NRIA (using realistic NN potentials) gives a fair description of all available  $t_{20}$  data.

Desplanques and Amghar [19] recently explored the possibility that some of the NN interaction models may be equivalent up to an unitary transformation. Quantities where the NN system couples to an external probe are affected by this transformation and should therefore be accordingly corrected. Once this is done, predictions made from different models tend to move closer to each other.

In the NRIA, the isoscalar nucleon electric form factor cancels in the ratio  $\alpha$  and therefore in  $\bar{t}_{20}$  (see Eqs. 2.15 and 2.16). In the NRIA,  $\bar{t}_{20}$  is strictly independent of  $G_E^n$ . Because its magnetic contribution is small,  $t_{20}$  is nearly independent of  $G_E^n$ . This will also be the case for all models which go beyond the NRIA.

#### 3.2 Meson-exchange currents and isobar contributions

Isoscalar meson exchange include pair and retardation currents, where the pion

contribution largely dominates over that of heavier mesons, as well as model-dependent  $\rho\pi\gamma$  and  $\omega\sigma\gamma$  contributions. Most MEC calculations include also various relativistic one- and two-body current contributions (RC) added perturbatively to the NRIA results.

As compared with NRIA, the minimum of  $G_C$  is shifted to lower  $Q$  values. This shift is larger than the Bates data would suggest, except in the case where the Bonn-E potential is used [13]. This trend is in apparent contradiction with similar calculations in the three-body system where the isoscalar charge form factor extracted from  $e\text{-}^3\text{He}$  and  $e\text{-}^3\text{H}$  elastic scattering [20] is better reproduced with the same MEC contributions as used for the deuteron [21].

Isobar degrees of freedom may be taken into account by adding to the wave function explicit  $\Delta\Delta$  and  $NN^*$  components. The deuteron form factors are then modified, both in the NRIA, with the assumption that the isobars have form factors proportional to those of the nucleons, and in the MEC calculation where additional terms must be taken into account. Present models [22, 23] predict isobar admixtures ranging from 0.36 to 7 %. However, the agreement with  $A$ ,  $B$  and  $t_{20}$  is worse for high  $\Delta\Delta$  components.

### 3.3 Relativistic calculations

Relativist calculations of the deuteron form factors can be divided into two general approaches [24]. Those based on the Bethe-Salpeter equation (BSE) are of the instant-form type while the front-form approach (also called light-cone quantum mechanics) is a type of Hamiltonian dynamics for a fixed number of particles where the matrix elements of the nucleon current operator and the nucleon electromagnetic form factors are related by kinematic transformations. Most relativistic calculations do not include contributions from MEC such as the  $\rho\pi\gamma$  process and are therefore referred to as relativistic impulse approximation (RIA). However the pair and retardation currents are included automatically in some models of RIA [25, 27]. Fully relativistic analysis of the  $\rho\pi\gamma$  and  $\omega\sigma\gamma$ , calculated consistently with the NN dynamics in the framework of a relativistic quasipotential one-boson-exchange model, have been done recently by Hummel and Tjon [28].

In order to achieve a manageable three-dimensional reduction of the BSE, various prescriptions have been used leading to different quasi-potential equations. The calculation of Arnold *et al.* [25] assumes that the spectator nucleon is on the mass-shell while the interacting nucleon is off-shell. A parameter  $\lambda$  can be varied between

0 (pure pseudo-vector) and 1 (pure pseudo-scalar) for the boson-nucleon couplings used to generate the wave function. Their results both for  $B(Q)$  and  $t_{20}$  are in favour of pure PV-coupling, when the RIA is closer to the NRIA.

Recently, Braun and Tokarev [45] undertook a similar calculation though with a different, allegedly more rigorous, treatment of the integrand in the form factors integrals. The agreement with  $t_{20}$  is however slightly worse.

Using another prescription, the wave function of the deuteron can be constructed by a combination of two functions, corresponding respectively to the case where the spectator, or struck, nucleon is on-shell [30]. This leads to a somewhat too small slope of  $t_{20}$ . The limit where only the spectator nucleon is on shell is in better agreement with the data, as in Arnold *et al.* [25].

Rupp and Tjon [31] obtained rigorous solutions of the BSE by using separable potentials. This class of potentials however, whether non-relativistically or in their covariant generalizations, misses the general features of the charge form factor: the node is shifted to  $Q$  values of about  $5.5 \text{ fm}^{-1}$ , much higher than the Bates experiment indicates.

Hummel and Tjon [28] have performed a relativistically covariant analysis of  $\rho\pi\gamma$  and  $\omega\sigma\gamma$  MEC, which were treated consistently with the NN dynamics within a quasipotential one-boson-exchange model. The perturbative treatment of MEC's in the non-relativistic approach neglects the recoil corrections due to the kinetic energy of the nucleons. This approximation is not justified at high momentum transfers. Hummel and Tjon derived the relativistic formulae for the  $\rho\pi\gamma$  and  $\omega\sigma\gamma$  current operators and evaluated their matrix elements using a relativistic OBE model with  $\pi, \rho, \omega, \sigma, \eta$  and  $\delta$  mesons. They find the  $\rho\pi\gamma$  contribution to the form factors to be much smaller than in the non-relativistic case, and consequently the  $\omega\sigma\gamma$ , thus far never considered, of comparable importance. The RIA is seen to be in perfect agreement with the data, while the addition of the MEC changes the results by less than one experimental error bar. The  $\rho\pi\gamma$  and  $\omega\sigma\gamma$  contributions to  $G_Q$  almost exactly cancel each other, while the  $\omega\sigma\gamma$  contribution to  $G_C$  is twice as large, with opposite sign, as the  $\rho\pi\gamma$  one. Similar relativistically covariant calculations have been performed by Devine [32], with equally good agreement with the existing data.

Relativistic models of front-form use the four-vector  $(t \pm z, x, y)$  as the kinematic variable, the four-momentum being then  $(E \pm p_z, p_x, p_y)$ . The equation of motion has a form similar to that of the non-relativistic Schrödinger equation, with a relativistic

wave function of the deuteron related to the non-relativistic one in a simple way:

$$\psi_{rel}(k) = (k^2 + M_d^2)^{1/2} \psi_{nonrel}(k) \quad (3.1)$$

Such calculation [33, 34] give a good description of the available data. The problem of including MEC has not yet been dealt within this approach.

### 3.4 Quark-hadron hybrid models

When electron scattering involves higher momentum transfers, the deuteron is probed at smaller internucleon distances. The quark substructure of the nucleons should then manifest itself in observables, but a distinct signature of quark effects in nuclei is still very elusive. Some calculations of the deuteron electromagnetic form factors explicitly take into account quark degrees of freedom. The deuteron structure is then described in hybrid models which mix quark and nucleon degrees of freedom.

The first class of such models assumes for the deuteron wave function a sum of two wave functions: a conventional NN wave function and a six-quark (6q) configuration, but does not contain any dynamics to link the hadronic and the 6q components. Kobushkin and Shelest [35] write  $\psi_d = \alpha\psi_{np} + \beta\psi_{6q}$  where  $\psi_{np}$  is calculated from the Reid hard core potential while  $\psi_{6q}$  is determined using a relativistic oscillator quark model. The six quarks are all considered to be in an S-state. The oscillator constant and the probability of the 6q admixture  $\beta^2$  were determined by fitting the then available data on  $A$  and  $B$ . They obtained  $\beta^2 = 2.5\%$ , but the 6q contribution to  $G_C$  is so large and positive that the node of this form factor disappears. This is in clear contradiction with the Bates data. Burov and Dostovalov [36] had a similar approach, with the difference that the 6q component was restricted to a small sphere of radius 1 fm and that MEC contributions (at the nucleon level) were included in the calculation of the form factors. Their 6q admixture was of 3.5% and  $G_C$  is also without a node. Cheng and Kisslinger [37] took into account five different six-quark configurations, also within the relativistic oscillator quark model. Their result differs widely from the work of Refs. [35, 36] since they do predict a node in  $G_C$  in the right  $Q$  range. Within these models, the form factors thus seem to be very sensitive to the six-quarks configurations being used.

A smooth dynamical connection between the configuration of two three-quark baryon clusters at long distances and a 6q configuration at short distance may be provided by the non-relativistic quark-cluster model (QCM), using the resonating group method. The QCM is able to reproduce the repulsive nature of the NN

interaction at short distances, but the intermediate range attraction is included through two-pion exchange or a phenomenological  $\sigma$  exchange. The long-range part of the interaction is given by OPEP between quarks. Yamauchi and Wakamatsu [38] demonstrated that it is rather ambiguous to speak about the  $6q$  components in the deuteron independently of their relation to the NN component. They calculate  $e$ - $d$  observables which are very close to the NRIA. Only in the magnetic form factor do quark effects manifest themselves through the antisymmetrisation of quarks between the two clusters. Quark exchange contributions to the form factors were also investigated [39, 40]: the impulse one-body current operators consist of a direct term (the coupling of the virtual photon to a quark in a cluster) and two exchange terms, where two quarks from different clusters are interchanged (the virtual photon then couples either to a spectator quark or to an interchanged quark). Buchman *et al.* [41] improved such calculations by including contributions from two-body pion and gluon exchange currents on the quark level. Quark exchange is found to have a small effect on  $t_{20}$ , so that, as in conventional calculations, the node of  $G_C$  is shifted to lower values of  $Q$  because of the  $\pi$  pair contribution.

### 3.5 Skyrme model

In the Skyrme model [42], baryons are identified with soliton solutions (Skyrmions) of a Lagrangian constructed on an  $SU(2)$  field  $U(\vec{r}) = \exp[i\vec{\tau} \cdot \hat{r} \vartheta(r)]$ .  $\tau$  is the nucleon isospin operator and  $\vartheta(r)$  is called the chiral angle, a function which satisfies an equation of motion of the underlying Lagrangian. The isoscalar electromagnetic current operator  $J^\mu$  is proportional to the anomalous baryon current operator which depends on the fields  $U$  of the Lagrangian but not on their interaction. Nyman and Riska [43] predicted the deuteron electromagnetic form factors within the Skyrme model adjusting  $\vartheta(r)$  to reproduce the isoscalar nucleon form factor, and representing the deuteron by a product *ansatz* of two soliton fields. As a result the current operator for the deuteron can be expressed as a sum of the isoscalar current operator of single nucleons and of an irreducible two-body exchange current operator. This exchange current in the Skyrme model has been formally identified [42] with the conventional  $\rho\pi\gamma$  MEC. The extended structure of the nucleons is taken into account automatically in the construction of the operators, so that no phenomenological cutoff form factors at the meson-nucleon vertices are needed. Nyman and Riska did not introduce any dynamics in the Skyrme model: the deuteron wave functions needed to calculate the matrix elements of the current operator  $J^\mu$  must be taken

from another dynamical model, and they chose to use the wave function generated conventionally from the Paris NN potential. Their results are in fair agreement with the Bates data although  $t_{20}$  is predicted to have a steeper slope than in most other models (see figure 1). Such a behaviour will be tested in the proposed experiment.

Braaten and Carson [45] consider the previous result as fortuitous: they criticized the product *ansatz* and the resulting additivity of the current operators. They calculated the deuteron form factors in the Skyrme model under the assumption that the deuteron should be identified with the ground state of the toroidal  $B = 2$  Skyrmion. All three form factors are then overestimated by an order of magnitude.

### 3.6 Perturbative quantum chromodynamics

At sufficiently large momentum transfer, PQCD is expected to become applicable. In elastic scattering, the deuteron keeps its identity, so that it is generally assumed that the momentum transfer is shared among the six quarks. Brodsky and collaborators [46] studied the high- $Q$  behaviour of the electromagnetic form factors of hadrons and of the deuteron within the framework of PQCD. Using the above assumption, they derived the so-called quark counting rule which predicts for the deuteron  $\sqrt{A(Q)} \propto Q^{-10}$  as  $Q \rightarrow \infty$ .

Carlson and Gross [47] showed that, though classical nuclear physics may lead to the same power law, spin observables could provide a distinctive signature of the domain of validity of PQCD: working in a helicity basis, the dominant matrix element of the electromagnetic current is the one where the deuteron has a 0 helicity in both initial and final states. This corresponds to a longitudinal form factor  $G_{L,00} = -\sqrt{Q^2 + 4M_d^2}[G_C + \frac{4}{3}\eta G_Q]$  which exhibits a  $Q^{-9}$  asymptotic behaviour. The double helicity flip term  $G_{L,+} = \sqrt{Q^2 + 4M_d^2}[G_C - \frac{2}{3}\eta G_Q]$  is suppressed by a factor  $Q^2$  compared to  $G_{L,00}$ , which leads, using Eqs. 2.15 and 2.16, to the prediction:

$$\lim_{Q \rightarrow \infty} \tilde{t}_{20} = -\sqrt{2}. \quad (3.2)$$

Carlson [48] later suggested that this asymptotic behaviour could be matched to the low transfer limit of Eq. 2.12 by the *ad hoc* construction:

$$G_C = (1/M_d^2 Q_d + \frac{2}{3}\eta)G_Q \quad (3.3)$$

The Bates data contradict this supposition, indicating that they are still far from the momentum transfer range where PQCD begins to be applicable.

Brodsky and Hiller [49] recently reexamined the question of asymptotic behaviour of the deuteron form factors: the relevant transfer momentum scale for the validity of PQCD is claimed to be  $Q \gg \sqrt{2M_d\Lambda_{QCD}} \sim 4.5 \text{ fm}^{-1}$ , which is much lower than the scale usually given by  $\eta \gg 1$ . The energy scale  $\Lambda_{QCD}$  is taken to be around 200 MeV. A calculation of the form factors in the light cone formalism [49, 50] keeping only the leading term  $G_{L,00}$ , results into :

$$G_C = (-1 + \frac{2}{3}\eta)G_Q \quad (3.4)$$

$$\bar{t}_{20} \simeq -\sqrt{2} \frac{\eta(\eta - 1)}{\eta^2 - \eta + \frac{3}{4}} \quad (3.5)$$

which in the limit  $\eta \gg 1$  leads to the Carlson and Gross prediction of Eq. 3.3. The present data are not incompatible with this behaviour as of  $Q \simeq 5 \text{ fm}^{-1}$ , but the assumption of the dominance of  $0 \rightarrow 0$  transition cannot account for the observed dip in the magnetic form factor [2]. A test of the applicability of PQCD to the description of the charge form factors will then be to determine whether  $t_{20}$  flattens out around zero above  $5 \text{ fm}^{-1}$ . Most other models predict that  $t_{20}$  will reach its absolute maximum ( $\bar{t}_{20} = 1/\sqrt{2}$  when  $x = -1/2$ ) around 6 or  $7 \text{ fm}^{-1}$ , while Eq. 3.4 predicts that this occurs at  $Q = 13.4 \text{ fm}^{-1}$ .

## 4 This experiment

The goal of this experiment is to extend to higher  $Q$  values the measurements of  $t_{20}$ . The preceding section illustrates that such data are needed, with good precision, to test validity of various models and to help choosing between different physical descriptions.

We have schematized the general experimental set-up in figure 2. This experiment will require two spectrometers for the detection of the scattered electron and recoiling deuteron in coincidence. The polarization of the recoiling deuterons will be measured in the polarimeter *POLDER*. The range of operation of this new polarimeter (i.e. 200–400 MeV deuteron energies) allows one to perform measurements in the range of four-momentum transfer  $Q$  starting from 4 and extending up to  $6.2 \text{ fm}^{-1}$  (see Eq. 2.1).

In this double scattering experiment, owing to the smallness of the  $e$ - $d$  cross-sections, an intense electron beam, a thick liquid deuterium target, large solid angles for the electron and deuteron spectrometers and a high efficiency for the deuteron polarimeter are needed to obtain a sufficient number of events.

For the liquid deuterium target, the 15 cm long cells being developed for CEBAF experiments will be needed. A high power cryogenic system must be associated with the target in order to allow the experiment to be performed at maximum beam intensity.

The experiment could be performed in Hall A or C of CEBAF using either the HRS or HMS spectrometers for the detection of the electron. For the deuteron magnetic channel, none of the existing spectrometers at CEBAF are really adapted for our case. Indeed very dispersive magnetic channels would lead to large spot of the recoiling deuterons on the polarimeter target and consequently to losses leading to a prohibitive beam time request. Thus we propose to develop a specific device (see following section) placed at a fixed angle.

### 4.1 The Deuteron Transport Channel

The purpose of the deuteron magnetic arm is to:

- i) give a deflection to the deuterons so that the polarimeter is not in direct view of the liquid deuterium target.
- ii) concentrate most of the deuterons associated with a detected electron in the electron spectrometer onto the polarimeter target. No particular resolution require-

ments are needed since, in this two-body reaction, the exact kinematics will be better determined by the electron spectrometer.

iii) Achieve a small deuteron spot since tensor polarization measurement may not be performed with an extended polarimeter. The present *POLDER* target cell is 10 cm in diameter; it could if needed be enlarged to a 16 cm diameter cell. But the larger the cell, the more the efficiency of the polarimeter will vary with the angle and position of the incoming deuterons.

iv) Help to eliminate most of background protons and pions produced in the  $LD_2$  primary target.

v) Identify deuterons by time of flight and momentum selection.

Existing spectrometers at CEBAF are too dispersive for our purpose since, even with modified optics, criterium iii) cannot be met. It has thus appeared worthwhile to propose to build a “simple” magnetic channel, set-up at a fixed angle, which could meet our requirements. Note that the solution of a specific deuteron channel was also the one adopted for the Bates experiment [10]. Our proposed design is a QQD system. The double bend used in the Bates experiment is not needed here because the proton and pion single rates on the polarimeter should be acceptable (see Section 6).

The acceptance of the deuteron channel has to match that of the electron spectrometer. The kinematical relations :

$$\frac{d\theta_d}{d\theta_e} = -\frac{\sin 2\theta_d}{2 \sin \theta_e} \quad (4.1)$$

$$\frac{d\phi_d}{d\phi_e} = -\frac{\sin \theta_d}{\sin \theta_e} \quad (4.2)$$

$$\kappa = \frac{1}{p_d} \frac{dp_d}{d\theta_d} \quad (4.3)$$

are, for a fixed four-momentum transfer  $Q$ , very rapidly increasing functions of the incident electron energy  $E_e$  (see figure 3) and will then lead to important factors of mismatch between the electron and deuteron spectrometers. Although the cross-section increases with energy, it is more advantageous not to introduce any mismatch between the deuteron and the electron arms and consequently not to work at the maximum energy.

We therefore optimized our design for the following conditions:

$Q = 6.2 \text{ fm}^{-1}$ ,  $T_d = 400 \text{ MeV}$ ,  $p_d = 1290 \text{ MeV}/c$ ,  $\theta_d = 53^\circ$ ,  $E_e = 2 \text{ GeV}$ . For these conditions, one gets, in order to match the HRS acceptance:

$$\theta_d^{max} = 0.75 \times \theta_e^{max} = \pm 23 \text{ mrad},$$

$$\kappa = -0.162 \text{ \%/mrad},$$

$$\phi_d^{max} = 1.24 \times \phi_e^{max} = \pm 80 \text{ mrad}.$$

In order to minimize the deuteron spot size, we imposed point to point focusing in the vertical direction and, in the horizontal (dispersive) plane, a condition of compensation of the kinematical change of momentum with angle:  $(x|\theta) + \kappa(x|\delta) = 0$ . The dipole must then bend toward the beam, as indicated on Figure 2. Figure 4 gives the trajectories originating from the extremities of the liquid deuterium target ( $\pm 4$  cm in projection) and with the maximum *correlated* angle and  $\delta$ . Because of the target size, one cannot avoid the large horizontal envelope in the second quadrupole. The spot size at the "focal" point is calculated by raytracing (in ideal fields so far) to be  $4 \times 4 \text{ cm}^2$  (see figure 5). This exceeds our initial requirement, but more detailed calculations, using field maps and including multiple scattering, are necessary.

Magnetic elements which could suit this design are available at Bates :

\* Q1: 8Q32, 1kG/cm (85 V, 1000 A).

\* Q2: rectangular aperture of  $15 \times 60$  cm and a length of 130 cm, 0.34 kG/cm (250 V, 440 A).

\* D: 10-15 cm gap, 18 kG over 1 m ( $25^\circ$  bend)

The whole QQD assembly, as well as a concrete hut around the polarimeter, will have to be supported at beam level.

Three collimators would be installed: the first one close to the target would eliminate particles originating from the target entrance and exit walls, the second at the entrance of the Q1 and the third one upstream of the polarimeter target.

## 4.2 Detection of the electron

The HRS (Hall A) and HMS (Hall C) spectrometers developed at CEBAF and their associated detection systems will be well adapted for our experiment. The time and energy information of the scattered electrons will be used in conjunction with the deuteron detection system to allow the rejection of background charged particles reaching the polarimeter. The connection of the information delivered by the 2 arms will have to be carefully studied at the acquisition level.

The deuteron detection angle being fixed, the electron spectrometer will be rotated to match the 2 body kinematics of the  $D(e, e' \vec{d})$  reaction (typically in the  $30\text{--}50^\circ$  domain).

### 4.3 Beam Energy and intensity

A large beam intensity is required in this experiment. Limitations could arise from the rate of background charged particles reaching the polarimeter and the power dissipated by the beam in the LD<sub>2</sub> target. A beam intensity of 100  $\mu$ A looks realistic and was considered for the background and beam time estimations (sections 6 and 7).

As the choice is made to perform the experiment at fixed deuteron angle, the beam energy will be changed for the different values of momentum transfer. Due to important kinematical mismatch factors (see figure 3), the choice has been made not to perform the experiment at the maximum beam energy. To a much lesser extent the radiative corrections and the power dissipated by the beam in the LD<sub>2</sub> target are also minimized with this choice. Calculations of kinematics and counting rates were made using the characteristics of the deuteron magnetic channel described in section 4.1 and the HRS spectrometer for the electron detection. We optimized the deuteron counting rates when placing the deuteron channel at an angle of 55°. Calculation of mismatch factors showed that the experiment should be performed with beam energies ranging from 1 to 2 GeV. The gains in cross-section one would get by increasing the beam energy are indeed balanced by the losses due to the non-matching of the solid angles of the electron and deuteron in the  $D(e, e' \vec{d})$  scattering.

### 4.4 The LD<sub>2</sub> target

We propose to use a cryogenic target developed for the CEBAF experiment in Halls A or C.

With a beam intensity of 100  $\mu$ A, the availability of a 500 W LD<sub>2</sub> target is crucial for this experiment, whether Hall A or C is used. The planned Hall A cryogenic system is thus adequate for this experiment. The beam will be either rastered or defocused in the horizontal direction on the target to avoid problems with local boiling.

The planned 15 cm length target cells of CEBAF are well adapted for this experiment. However the target windows will be collimated in order to reduce the background in both spectrometer arms. This will then lead to a useful length of about 10 cm.

## 5 Polarization Measurement

One key element of the experiment is the polarimeter which measures the polarization of the recoiling deuteron.

A polarimeter requires a nuclear reaction to have both large analysing powers and cross sections in order to yield measurable asymmetries with respect to the incident particle polarizations. The cross section for such a reaction depends upon the incident polarization through [51] :

$$\sigma(\theta, \phi) = \sigma_0(\theta) [1 + t_{20} T_{20} + 2(it_{11} iT_{11} + t_{21} T_{21}) \cos(\phi) + 2t_{22} T_{22} \cos(2\phi)] \quad (5.1)$$

where  $T_{kq}$  are the analysing powers of the reaction and  $t_{kq}$  the polarization coefficients of the particles. Here  $\sigma_0$  is the cross section for unpolarized incident deuterons and  $\phi$  the angle between the normals to the reaction and the e-d scattering planes.

Unpolarized cross section and analysing powers ( $\sigma_0$  and  $T_{kq}$ ) have first to be measured in calibration runs with beams of known polarization. Only then can the polarimeter being used to measure polarisation of incident particles from the experimental asymmetries measured with the polarimeter operated with exactly the same cuts and efficiencies of the calibration run.

Finally, polarimeters are characterized by a so-called figure of merit given by

$$(F_{kq})^2 = \int (T_{kq})^2 \epsilon(\Omega) d\Omega \quad (5.2)$$

where  $\epsilon$  is the ratio of the number of reactions to the number of incident particle ( $N_{incident}$ ) and  $T_{kq}$  the analysing powers of the analyzing reaction. These quantities are integrated over the phase space covered by the polarimeter. The figure of merit allows one to compare different competing apparatus because it governs the statistical error made in a polarimeter measurement through the following relation :

$$\Delta t_{kq} = \left( F_{kq} \sqrt{N_{incident}} \right)^{-1} \quad (5.3)$$

From this, one sees that the larger the figure of merit, the smaller the error for a given number of incident particles (and thus of beam time).

### 5.1 The *POLDER* Polarimeter

*POLDER* is based on the  $^1\text{H}(\vec{d}, 2p)n$  reaction as proposed by Bugg and Wilkin [52]. Their predictions have been checked in experiments performed at 200 and 350 MeV

[53] and a fair agreement was found between the theory and the data. At 200 MeV the figures of merit ( $F_{20}$  and  $F_{22}$ ) in the  ${}^1\text{H}(\vec{d},2\text{p})\text{n}$  [53] reaction were found to be comparable to those of the  ${}^1\text{H}(\vec{d},\text{p})\text{X}$  reaction used in the *AHEAD* polarimeter [9]. However the crucial feature of the  ${}^1\text{H}(\vec{d},2\text{p})\text{n}$  reaction is that its figures of merit remain large up to at least 350 MeV whereas those of the  ${}^1\text{H}(\vec{d},\text{p})\text{d}$  reaction fall quickly above 200 MeV [54]. The figure of merit  $F_{11}$  for the vector analyzing power is zero for this reaction. Also the  ${}^1\text{H}(\vec{d},2\text{p})\text{n}$  reaction is well understood in terms of the impulse approximation [55], and theoretical predictions can thus be used for numerical simulations.

The experimental set-up (see figure 6) has been constructed by a collaboration of the Institut des Sciences Nucléaires of Grenoble and the Laboratoire National Saturne at Saclay.

The measurement of the directions and impact points of incident deuterons on the target is performed with good precision by two multiwire proportional chambers (MWPC1/2) placed upstream of the target. These are composed of two planes providing X and Y information and constituted of wires separated by 1 mm. The MWPC's are operated with a standard magic mixture and efficiencies of 95 % per plane were obtained for deuterons of interest (200–400 MeV). These detectors are capable of detecting multi-hit events, thus permitting the rejection of two-charged-particles events originating from upstream of the target.

The measurement of the number of deuterons incident on the target, necessary for the cross section normalisation, is determined by a coincidence in two detectors (S1 and S2) composed of thin fast plastic (NE102) scintillators (300  $\mu\text{m}$  thick and 8 cm in diameter) optically coupled to two phototubes (XP2020). The coincidence signal from these two detectors achieves a clean rejection of false events generated by background particles and/or electronic noise and is also used for the start signal of the time-of-flight measurement of the protons produced in the reaction. The total dead time of the experiment vetoes this coincidence and so exactly the same correction is applied to the measured number of reactions and incident deuterons. The information delivered by the electron spectrometer will be used in conjunction with those of *POLDER* to ensure the discrimination of incident deuterons against the background particles reaching *POLDER*.

The  ${}^1\text{H}(\vec{d},2\text{p})\text{n}$  reaction takes place in a liquid hydrogen ( $\text{LH}_2$ ) target of cylindrical shape, 16 cm long and 10.2 cm in diameter. The target cell is made of 170  $\mu\text{m}$  thick mylar with an entrance window of 120  $\mu\text{m}$  thick kapton. This is mounted

in a vacuum chamber with entrance and exit windows made of titanium of 50 and 100  $\mu\text{m}$  thickness. The target is operated at a temperature of 17.5°K, controlled by a monitoring system, with a 10 W cryogenic system. Changes are foreseen to comply with the US safety regulations for enclosed liquid target operation.

The protons created in the  ${}^1\text{H}(\vec{d},2\text{p})\text{n}$  reaction are detected in two hodoscopes placed after the target, as shown in figure 6. The solid angles covered by this pair permit, with good efficiency, the detection of protons from the  ${}^1\text{H}(\vec{d},2\text{p})\text{n}$  reaction in the range of momentum transfer to the neutron (q) where most of the cross section of the  ${}^1\text{H}(\vec{d},2\text{p})\text{n}$  reaction is located. The hodoscopes are formed of two planes providing X and Y information and the thicknesses of the scintillators (0.2 cm and 1 cm) were kept small in order to reduce the reaction rate in the detectors. Dead areas have been minimized and detection efficiency for two-particle events is about 90 %. The plastic bars are optically coupled to a phototube at only one extremity. The information on the numbers of the bars fired in the two hodoscopes permits one to determine the directions of the protons. To achieve this, the first hodoscope is rotated by 45° to remove ambiguities in the determination of the directions of the protons. At our energies, the characteristics and kinematics of the  ${}^1\text{H}(\vec{d},2\text{p})\text{n}$  reaction allow one to discriminate charge exchange events from other parasitic reactions by the simple condition that two charged particles are detected at velocities close to those of the incident beam. As the thin plastic scintillators making up *POLDER* are mostly sensitive to charged particles, no particle identification is necessary. The velocity of the detected particles is obtained by a time of flight measurement and energy measurements are therefore not necessary. These features simplify considerably the operation of the apparatus and reduce gating problems in data treatment.

Finally a veto detector is placed on the beam axis. This detector is composed of an absorber which stops the protons of interest and of a plastic scintillator coupled to two phototubes which detects the deuterons. This veto detector allows then to reject background events associated with the detection of at least one of the incident deuterons.

A VME acquisition system is associated with the set-up and based on 68030 microprocessors running in parallel for data acquisition, recording, on-line control and calculations. The times of flight of the particles are recorded as well as the numbers of the bars which fired in each hodoscopes. The signal delivered by the MWPC are treated by a fast digital read-out system which can handle multi-hit events and information are obtained for each track. Data are recorded on exabyte

tapes and the acquisition uses CAMAC standard for data encoding (TDC, scaler, pattern unit). Using the pattern unit information, only the TDC values of fired detectors are recorded allowing gains of space on tapes. This system ( which will be upgraded with 68040 microprocessors) can handle more than 300 events per second with small dead time. This is sufficient in our case as the expected acquisition rate will only be of some tens of events per second in this experiment. The information from the electron spectrometer will be used to reject background events and have also to be recorded. The interconnection of both electronics and acquisition systems will be studied with the collaboration of the Hall of choice. An Ethernet link is finally used to send data to a workstation for on-line control, sophisticated event selections, fits and plotting. In particular, preliminary deuteron polarization can be calculated during the experiment.

## 5.2 Calibration of the Polarimeter

The polarimeter was calibrated in May 1992 for incident deuteron energies of 300 and 380 MeV and a second calibration run is scheduled next July to complete this set of data with measurements at 200, 250 and 350 MeV.

The calibration experiments have been performed using the polarized deuteron beams delivered by the Saturne synchrotron which can provide deuterons of known (with a 2–3% accuracy [56]) vector and tensor polarization. The polarimeter *POLDER* was installed in the focal plane of the spectrometer SPES1. In order to measure the  $T_{21}$  analyzing power, a superconducting solenoid was used to rotate the spin axis of the beam by  $90^\circ$  from the vertical to the horizontal plane in conjunction with the SPES1 spectrometer acting as a dipole magnet. For consistency checks, the measurements were performed both with and without the solenoid.

### 5.2.1 Data Handling and Background Rejection

The selection of the pp pairs originating from the  $^1\text{H}(\vec{d}, 2\text{p})\text{n}$  reaction is performed using a limited number of gates. Most of the background events, which reduce the polarization signal and contribute to the cross section in a non-reproducible way, are rejected using the time-of-flight information on the detected particles from the second hodoscope.

Precise time-of-flight data ( $\leq 1$  ns FWHM) are obtained after corrections for the transit time of the light in the bars. As the two protons created in the  $^1\text{H}(\vec{d}, 2\text{p})\text{n}$

reaction have very similar velocities, another gate was set on the difference in the corrected times of flight.

The mechanical alignment for all the elements of the set-up is obtained from an off-line procedure which uses the individual counting rates of the bars of the hodoscopes and the beam axis defined by the MWPC's. This alignment uncertainty mostly influences the  $t_{21}$  determination and a systematic error of about 0.05 has to be considered for the measurement of this quantity according to the precision of the alignment deduced from the data analysis. This should be improved by using a third MWPC placed close to the veto detector.

The direction of the two protons is fixed by the numbers of the bars which fire in the two hodoscopes, whereas the incident particle direction is measured in the two MWPC's placed before the target. From these one can determine the direction of the centre-of-mass of the pp pair and the polar angle  $\theta$  (closely related to the momentum transfer  $q$  to the neutron) as well as the azimuthal angle  $\phi$  information. As large tensor signals are only found for small excitation energies of the pp pair ( $E_x \leq 8$  MeV) [53], this quantity is derived from our data by using the relative angles of the two protons combined with their time of flight.

Using the directions of the incident deuteron and those of the two protons, it was possible to calculate the vertex of the reaction by a fitting procedure. This enables us to make a clean discrimination between events originating from the target and those created elsewhere (mostly the plastic bars of the first hodoscope).

Data obtained from all this treatment were compared with the results of a simulation program which physics inputs are the full predictions of the impulse approximation model [55] filtered by the experimental device and with the same cuts. Figure 7 shows the fair agreement between data measured at ( $T_d = 380$  MeV) and simulation for two keys quantities of this experiment (the excitation energy of the pp pair  $E_x$  and momentum transfer  $q$ ). Since the theory has been previously checked with a different detector, this result gives confidence in the data handling and background rejection.

### 5.2.2 Analysing Power and Cross Section Determination

The counting rates for the  ${}^1\text{H}(\vec{d}, 2p)n$  reaction events, binned in  $q$  and  $\phi$ , is measured for different beam polarizations and combined, for the same number of deuterons, to construct vector and tensor asymmetries. The sum of these normalized yields ( $N_i$ ) provides the counting rate for an unpolarized beam. The tensor

analysing powers  $T_{20}$ ,  $T_{21}$  and  $T_{22}$ , which are related to the asymmetries, are deduced using a  $\chi^2$  minimisation procedure.

For the  $t_{20}$  measurements, the absolute values of the unpolarized cross sections must be very well known and thus many different experimental conditions have been tested. In particular the dependence of the results on the beam intensity and direction was examined. It appears that the unpolarized cross section deduced from these measurements in different runs, after all cuts in the off-line treatment, were stable and mutually compatible within statistical errors as illustrated in figure 8. Systematic errors were estimated to be less than 0.5% for the unpolarized cross-section in our set-up and data treatment.

The results obtained at  $T_d = 380$  MeV for a cut of 5 MeV on  $E_x$  are displayed in figure 9 with statistical errors only. Uncertainties due to the beam polarization measurement were estimated to be less than 3%. The full curves are the predictions of the impulse approximation model with a cut at 8 MeV which can only be used for qualitative comparisons since the cuts are not matched. The experimental cross sections have not been corrected for geometrical detection efficiencies in the hodoscopes and the rapid fall above 250 MeV/c indicates an increasing effect occurring in *POLDER* at large detection angles. The data for  $T_{20}$  and  $T_{22}$  obtained with and without  $T_{21}$  contributions are consistent and typical statistical errors of better than 5% were reached around 120 MeV/c. Also, as shown in figure 9, the data exhibit a very smooth dependence with  $q$ . The vector signal ( $iT_{11}$ ) is consistent with zero, whereas  $T_{21}$  values are somewhat larger than expected.

Broadly similar conclusions can be drawn from the 300 MeV data displayed in figure 10, though it should be noted that cross sections becomes higher as the beam energy decreases leading to larger figures of merit. Measurements are scheduled to complete the calibration data at 200, 250 and 350 MeV.

The integrated figures of merit, taking into account all efficiencies (MWPC, detections, cuts, etc.), are given in table 1. For the 200 MeV energy, extrapolation, based on our previous study of the  ${}^1\text{H}(\vec{d}, 2\text{p})\text{n}$  reaction [53], is made for the beam time estimate.

Table 1 :

Figures of merit  $F_{kq}$  measured at  $T_d = 300$  and  $380$  MeV with *POLDER*. These have been calculated with  $E_x \leq 5$  MeV.

$T_d$ (MeV)	$F_{20}$	$F_{21}$	$F_{22}$
380	0.0075	0.005	0.009
300	0.01	0.0065	0.0095

### 5.3 Deuteron Polarization Measurements

Knowing the unpolarized cross section and analysing powers ( $T_{kq}$ ) of the  ${}^1\text{H}(\vec{d}, 2\text{p})\text{n}$  reaction from calibration runs, the asymmetries in counting rates allow one to determine the incident particles polarization tensors. The experimental asymmetries measured in *POLDER* are given by :

$$\begin{aligned}
 N(q, \phi) = & kN_0(q)(1 + 2it_{11}i T_{11}(q)\cos(\phi) + t_{20}T_{20}(q) \\
 & + 2t_{21}T_{21}(q)\cos(\phi) + 2t_{22}T_{22}(q)\cos(2\phi))
 \end{aligned}
 \tag{5.4}$$

A  $\chi^2$  minimization procedure is used to calculate the polarization tensors of the deuterons ( $t_{kq}$ ) from the  $q$  ( $\theta$ ) and  $\phi$  dependence of this cross section. All geometrical and detection efficiencies are in principle contained in the unpolarized cross section measured during the calibration run, but an overall normalizing factor  $k$  may be needed. Now there is a very strong correlation between the values of the cross section and  $t_{20}$  polarization and this leads to large systematic errors if the  $k$  factor is left completely free. This is far less important for the  $t_{22}$  and  $t_{21}$  which are defined mainly by their  $\phi$  dependence. Fortunately the calibration runs have shown that it is possible to fix  $k$  to within 1 %. As the value of the average  $T_{20}$  lies around 0.2, this lead to typical systematic errors of 0.05 which will have to be added to the statistical error deduced from the figures of merit as given by relation 5.3.

A sample of data recorded during the calibration run has been selected and analyzed following the procedure described above. This allows for checks of the ability of *POLDER* to be operated in polarimeter mode and for the study of the errors associated with the statistics recorded during the calibration, polarization measurement runs, and with the fitting procedure. The polarizations extracted from the fitting procedure were compared with those measured at low energy by the means of a polarimeter prior to the acceleration stage. For all three tensor

polarization ( $t_{20}$ ,  $t_{21}$ ,  $t_{22}$ ), results fairly agreed within the error bars as shown in figure 11. Systematic error due to the statistics of the calibration (of the order of 0.02) are combined with statistical errors in the data. Typical systematic errors of 0.05 have also to be considered and added.

The systematic errors, compiled in table 2 for the 380 MeV run, are of two types. First those linked to statistical errors associated to the calibration run. Secondly, additional systematic errors for  $t_{20}$  linked to the correlation between parameters  $k$  and  $t_{20}$  and the associated error of the unpolarized cross section. For  $t_{21}$  a systematic error is due to the alignment uncertainty. Systematic errors become large when very small statistics are used ( $\leq 10^6$  incident deuterons).

Table 2 :

Statistical and systematic errors measured at  $T_d = 380$  MeV with *POLDER* .

N deuterons	Polarization tensors	Statistical error	Systematic error (calibration)	Systematic error (others, see text)
4 $10^6$	$t_{20}$	0.07	0.012	0.06
	$t_{21}$	0.07	0.017	0.05
	$t_{22}$	0.037	0.004	negligeable

Finally one can mention that *POLDER* was also used to measure signatures of isoscalar spin-flip transitions in  $A(\vec{d}, \vec{d}')A^*$  scattering [57]. The preliminary results are in agreement with expected theoretical (in elastic scattering) or previously measured (for inelastic) values.

## 6 Estimate of Background Rate

From the polarimeter information and the requirement of the coincident detection of the electron, the incident deuterons and true charge exchange events should easily be discriminated against background particles and associated events.

However, it is important to perform simulations to estimate the single counting rates of background charged particles (protons, pions...) endured by the polarimeter. If this rate is too large, this may perturb the measurement or the proper operation of the detectors. For this purpose, we are using a code developed at CEBAF for CLAS which takes into account many processes (electro- and photo-excitation and subsequent decay of nucleonic resonances, quasi-elastic scattering, ...) [58]. The photo-disintegration of the deuteron, which is a serious source of background, is now also available from the simulation [59].

The simulation has been made for three beam energies. The 1 to 2 GeV range corresponds to this experiment, whereas the 0.5 to 1 GeV one is close to the range of the Bates experiment [10]. Four different processes have been studied at this moment : the photo and electro-production of  $\Delta$  and  $N^*$  resonances, the quasi-elastic process (including the effect of Fermi motion) and the photo-disintegration of the deuteron. The production rates of protons and pions have been investigated and preliminary results are shown in figures 12 and 13 for protons (pions being much less produced at combination of momentum and angles allowing their detection in the polarimeter). These figures show that only a small fraction of the particles produced in electro and photo-production of resonances can reach the polarimeter (see figure 13). Estimates of single counting rates have still to be performed, but figure 12 shows that viable experimental conditions should be obtained. Indeed at 1 GeV, experimental conditions look close to those of the high energy point of Bates. The background rate is much larger for our lower beam energies, but in this case as the deuteron rate is large, the beam intensity could eventually be reduced.

This work is still in progress. More detailed studies as a function of beam energy and deuteron detection angle are underway and single rates in the deuteron and electron arms will be estimated.

## 7 Beam Time

In this section we will detail our beam time estimate and associated errors given in table 3.

### 7.1 Counting Rates

The cross section is calculated using relation 2.4 with a fixed angle of  $55^\circ$  for the deuteron spectrometer. The beam energy and electron angles for each value of momentum transfer  $Q$  to the deuteron are calculated from a 2 body relativistic kinematics. The solid angles considered here are those of the HRS spectrometer and of the deuteron channel described in section 4.1. The deuteron spectrometer characteristics and the detection angles and beam energies chosen for this experiment avoid any kinematical mismatch.

The values of the structure functions  $A(Q^2)$  are interpolated from the values of reference [1], and  $B(Q^2)$  can be neglected in our case. It should be noted that the accuracy of the data for  $A(Q^2)$  in this  $Q$  domain has to be improved with new measurements.

A beam intensity of  $100 \mu\text{A}$  and an useful target length of 10 cm (collimators being used to remove the background events produced in the target entrance and exit windows) will yield a luminosity of  $3 \cdot 10^{38} \text{ cm}^{-2}\text{s}^{-1}$ . The radiative corrections have been estimated. In our case the coincidence between the deuteron and electron arms in this 2 body reaction should prevent the detection of background events. Thus the window set on the electron energy spectra can be loose and consequently the loss of events due to the radiative emission is weak. The limiting factor here is the momentum acceptance of the electron spectrometer. A loss of 20 % (calculated with a realistic 100 MeV wide window) is considered in our case. This correction is calculated for beam energies ranging in the 1–2 GeV domain and increases with increasing beam energy.

### 7.2 Beam Time and Statistical Accuracy

The statistical precision of the  $t_{20}$  measurement is estimated from the polarimeter figures of merit (relation 5.3) measured in calibration. One will have to add systematic errors which are due to the correlation between the absolute normalization and  $t_{20}$  (estimated to be of the order of 0.05), the precision in the mechanical alignment (for  $t_{21}$ , about 0.05) and also the statistics recorded during the calibration runs

(estimated to be less than 0.02 for  $10^8$  deuterons).

**Table 3 :**

Beam time and associated statistical errors in the measurement of  $t_{20}$ . The calculation is performed with a beam intensity of  $100 \mu\text{A}$ , a target length of 10 cm and a radiative loss factor of 0.8. The deuteron angle is fixed at  $55^\circ$  with no mismatch factor. Systematic errors, which have to be added, are estimated to be about 0.06.

$Q$ ( $\text{fm}^{-1}$ )	$T_d$ (MeV)	$E_e$ (GeV)	$\theta_e$ ( $^\circ$ )	$A(Q^2)$ (SLAC)	Time (days)	N deuterons	$F_{20}$	$\Delta t_{20}$
4.4	200.	1.15	46.	$2 \cdot 10^{-4}$	2	$8.5 \cdot 10^6$	0.013	0.03
5.0	260.	1.5	42.2	$6.5 \cdot 10^{-5}$	5	$6.2 \cdot 10^6$	0.011	0.04
5.6	330.	1.85	39.	$2.5 \cdot 10^{-5}$	15	$6.5 \cdot 10^6$	0.009	0.05
6.2	400.	2.2	35.5	$2 \cdot 10^{-5}$	15	$4.5 \cdot 10^6$	0.0075	0.07

From table 3, it appears that within 6 weeks of beam time, it will be possible to significantly improve the precision of the point measured at Bates around  $4 \text{ fm}^{-1}$  and measure 3 new points with a good accuracy up to  $6.2 \text{ fm}^{-1}$  (see figure 1).

### 7.3 Beam Time Request and Schedule

Preliminary beam time periods will also be required for tests, background reduction and counting rates checks. Also time is needed for beam energy changes. Finally we estimate that a one-month period will be necessary for installation of the polarimeter and deuteron channel. This lead to the following beam time request and schedule:

<b>Preparation</b>	160 hours
<b>Physics</b>	900 hours
<b>Contingency</b>	<u>140 hours</u>
	1200 hours

We will be ready to install the experiment by the end of 1996. Ideally the schedule for the experiment would be :

<b>Installation</b>	1 month
<b>followed by preparatory tests</b>	one week
<b>1 month later</b>	2 weeks at $Q=4.4, 5.0, 5.6 \text{ fm}^{-1}$
<b>4 months later</b>	3 weeks at $Q=5.6, 6.2 \text{ fm}^{-1}$

## 8 Comparison with other experiments

The recoiling deuteron polarization measurement, as proposed here, has so far [10] been the most efficient way to measure  $t_{20}$  and the proposed experiment will improve significantly on the overall figure of merit of the experiment performed recently at Bates.

An alternate technique to measure the same quantity is to scatter electron off a polarized target. In this case one deals with single scattering experiments and only analyzing power ( $T_{20}$ ) has to be measured. Experiments based on an external cryogenic polarized target are very limited by the amount of beam this kind of target can withstand [8]. Even if used with large acceptance detectors, it is presently not competitive with the polarimeter technique. Another method has been pioneered at Novosibirsk [5, 6] using an internal target in a storage ring. Target technology is progressing steadily [7] and using a high energy machine (in order to gain in cross section) new viable experiments may be performed in several years [60].

In table 4, we have compared the performance of different, already performed or proposed, experiments. Table 4.a shows the comparison of experiments based on polarimeters and table 4.b those based on polarized targets.

Table 4.a : Comparison of recoiling deuteron polarisation experiments.

Experiment	D <sub>2</sub> O + polarimeter Bates [4]	LD <sub>2</sub> + polarimeter Bates/AHEAD [10]	LD <sub>2</sub> + polarimeter CEBAF/POLDER (this proposal)
Beam energy (GeV)	0.371	0.85	2.0
Beam intensity ( $\mu$ A)	30	30	100
Target density (at/cm <sup>2</sup> )	$4.2 \times 10^{21}$	$2.4 \times 10^{23}$	$4.8 \times 10^{23}$
Luminosity (cm <sup>-2</sup> s <sup>-1</sup> )	$7.9 \times 10^{35}$	$4.5 \times 10^{37}$	$3. \times 10^{38}$
e <sup>-</sup> solid angle (msr)	20	18	7
Losses	0.5	0.25	0.2
Polarimeter efficiency $\epsilon$	$10^{-4}$	$2. \times 10^{-3}$	$1.6 \times 10^{-3}$
Analysing Power $T_{20}$	-0.8	-0.4	-0.2
Figure of merit $F = L\Omega\epsilon T_{20}^2 E^2$	$6.9 \times 10^{28}$	$4.7 \times 10^{31}$	$4.3 \times 10^{32}$
$Q_{max}$ (fm <sup>-1</sup> )	2.0	4.6	6.2

Table 4.b : Comparison of polarized target experiments.

Experiment	Polarised ND <sub>3</sub> Bonn [8]	Internal polarised atomic beam Novosibirsk [7]	Internal cell optical pumping + spin exch. HERA-HERMES (being considered)
Beam energy (GeV)	2.	2.	10.
Beam intensity	0.4 nA	200 mA	60 mA
Target density (at/cm <sup>2</sup> )	$9 \times 10^{22}$	$6 \times 10^{11}$	$10^{15}$
Luminosity (cm <sup>-2</sup> s <sup>-1</sup> )	$2.3 \times 10^{32}$	$7.5 \times 10^{29}$	$3.8 \times 10^{32}$
e <sup>-</sup> solid angle (msr)	5	120	120
Target polarization $A/\sqrt{2}$	0.12	0.46	0.6
Figure of merit $F = L\Omega\epsilon A^2 E^2$	$6.5 \times 10^{28}$	$7.8 \times 10^{28}$	$1.6 \times 10^{33}$
$Q_{max}$ (fm <sup>-1</sup> )	3.6	2.9	6.

From this, one can stress that the combination of the CEBAF facility and of the *POLDER* polarimeter constitute, at the present time, the most competitive tool for  $t_{20}$  measurement.

## 9 Status of the Collaboration. Distribution of the tasks

This proposal was handed to Halls A or C Leaders and Co-Program Managers, in order to explore the interest of both the collaborations in this project. Also the technical aspects that may dictate the final choice of the Hall has to be further investigated and the participation of groups involved in the cryogenic target, electron spectrometer and data acquisition are mostly wanted.

At the present time the collaboration is not yet finalized and a more definite status will be presented at the next PAC meeting in June. What can be stated at this stage is the following:

**Polarimeter** : Grenoble-Saclay-Orsay-Saturne. Final tests and calibration of the polarimeter. This could involve changes in either the  $\text{LH}_2$  or detection device. MIT/Bates might be involved in the safety aspect of the target.

**Deuteron channel** : Saclay-MIT/Bates. SNPI/Gatchina has expressed interest into a participation.

**$\text{LD}_2$  Target** : CEBAF/Univ. of Maryland/Basel

**Electron spectrometer** : CEBAF/Rutgers

**Data acquisition** : Grenoble/CEBAF/Rutgers. (In particular the interconnection of the acquisition systems of *POLDER* and electron spectrometer).

## References

- [1] R.G. Arnold *et al.*, Phys. Rev. Lett. **35**, 776 (1975);  
S. Platchtkov *et al.*, Nucl. Phys. **A510**, 740 (1990).
- [2] S. Auffret *et al.*, Phys. Rev. Lett. **54**, 649 (1985);  
P.E. Bosted *et al.*, Phys. Rev. C **42**, 38 (1990).
- [3] M. Garçon, Nucl. Phys. **A508**, 445c. (1990).
- [4] M.E. Schulze *et al.*, Phys. Rev. Lett. **52**, 597 (1984).
- [5] V.F. Dmitriev *et al.*, Phys. Lett. **157B**, 143 (1985).
- [6] B.B. Voitsekhovskii *et al.*, JETP Lett. **43**, 733 (1986).
- [7] R. Gilman *et al.*, Phys. Rev. Lett. **65**, 1733 (1990).
- [8] B. Boden *et al.*, Z. Phys. C - Part. and Fields **49**, 175 (1991).
- [9] J.M. Cameron *et al.*, Nucl. Inst. and Methods **A305**, 257 (1991).
- [10] I. The *et al.*, Phys. Rev. Lett. **67**, 173 (1991);  
M. Garçon *et al.*, Preprint CEA, (1993), unpublished.
- [11] G.E. Brown and A.D. Jackson, *The Nucleon-Nucleon Interaction*, North-Holland Publishing, (Amsterdam, 1976).
- [12] R. Machleidt, K. Holinde and Ch. Elster, Phys. Rep. **149**, 1 (1987).
- [13] J. Pauschenwein, W. Plessas and L. Mathelitsch, Few-Body Systems, Suppl. **6**, 195 (1992).
- [14] M.I. Haftel, L. Mathelitsch, and H.F.K. Zingl, Phys. Rev. C **22**, 1285 (1980).
- [15] V.M. Muzafarov and V.E. Toitskii, Sov. J. Nucl. Phys. **33**, 783 (1981).
- [16] I.I. Belyantsev, V.K. Mitrjushkin, P.K. Rashidov, and S.V. Trubnikov, J. Phys. G: Nucl. Phys. **9**, 871 (1983).
- [17] B. Mosconi and P. Ricci, Few-Body Syst. **6**, 63 (1989); *Erratum, ibid.* **8**, 159 (1990).
- [18] R. Schiavilla and D.O. Riska, Phys. Rev. C **43**, 437 (1991).
- [19] B. Desplanques and A. Amghar, Z. Phys. - Hadrons and Nuclei **A344**, 191 (1992).
- [20] A. Amroun *et al.*, Phys. Rev. Lett. **69**, 253 (1992).

- [21] R. Schiavilla, V.R. Pandharipande and D.O. Riska, *Phys. Rev. C* **41**, 309 (1990);  
H. Henning, J. Adam, Jr. and P.U. Sauer, *Few-Body Systems, Suppl.* **5**, 133  
(1992).
- [22] R. Dymarz and F.C. Khanna, *Nucl. Phys.* **A507**, 560 (1990).
- [23] P.G. Blunden, W.R. Greenberg, and E.L. Lomon, *Phys. Rev. C* **40**, 1541 (1989).
- [24] P.A.M. Dirac, *Rev. Mod. Phys.* **21**, 392 (1949).
- [25] R.G. Arnold, C.E. Carlson, and F. Gross, *Phys. Rev. C* **21**, 1426 (1980).
- [26] F. Gross, in *Modern topics in electron scattering*, B. Frois & I. Sick eds, World  
Scientific (Singapore 1991);  
J.A. Tjon, in *Hadronic Physics with multi-GeV electrons*, B. Desplanques and  
D. Goutte eds., Nova Science (New-York 1991).
- [27] M.J. Zuilhof and J.A. Tjon, *Phys. Rev. C* **24**, 736 (1981); *Phys. Rev. C* **22**,  
2369 (1980).
- [28] E. Hummel and J.A. Tjon, *Phys. Rev. C* **42**, 423 (1990).
- [29] M.A. Braun and M.V. Tokarev, *Sov. J. Part. Nucl.* **22**, 601 (1991).
- [30] R. S. Bhalerao and S. A. Gurvitz, *Phys. Rev. Lett.* **47**, 1815 (1981).
- [31] G. Rupp and J.A. Tjon, *Phys. Rev. C* **41**, 472 (1990).
- [32] N. Devine, Ph.D. thesis, University of Maryland, 1992, unpublished;  
and private communication.
- [33] L.L. Frankfurt, *et al.* *Phys. Rev. Lett.* **62**, 387 (1989).
- [34] P.L. Chung, *et al.* *Phys. Rev. C* **37**, 2000 (1988).
- [35] A.P. Kobushkin and V.P. Shelest, *Sov. J. Part. Nucl.* **14**, 483 (1984).
- [36] V.V. Burov and V.N. Dostovalov, *Z. Phys. A - Atomic Nuclei* **326**, 245 (1987).
- [37] T-S. Cheng and L.S. Kisslinger, *Phys. Rev. C* **35**, 1432 (1987).
- [38] Y. Yamauchi and M. Wakamatsu, *Nucl. Phys.* **A457**, 621 (1986).
- [39] H. Ito and A. Faessler, *Nucl. Phys.* **A470**, 626 (1987).
- [40] H. Ito and L.S. Kisslinger, *Phys. Rev. C* **40**, 887 (1989).
- [41] A. Buchman, Y. Yamauchi and A. Faessler, *Nucl. Phys.* **A496**, 621 (1989).

- [42] T.H.R. Skyrme, Nucl. Phys. **31**, 556 (1962);  
E. Witten, Nucl. Phys. **B223**, 422 (1983).
- [43] E.M. Nyman and D.O. Riska, Nucl. Phys. **A468**, 473 (1987).
- [44] M. Wakamatsu and W. Weise, Nucl. Phys. **A477**, 559 (1988).
- [45] E. Braaten and L. Carson, Phys. Rev. D **39**, 838 (1989).
- [46] S.J. Brodsky, Comments Nucl. Part. Phys. **12**, 213 (1984); and references therein.
- [47] C.E. Carlson and F. Gross, Phys. Rev. Lett. **53**, 127 (1984).
- [48] C.E. Carlson, Nucl. Phys. **A508**, 481c (1990).
- [49] S.J. Brodsky and J.R. Hiller, Phys. Rev. D **46**, 2141 (1992).
- [50] F. Coester, Proc. Int. Conf. Medium- and High-Energy Nuclear Physics, Taipei, Taiwan, 1988, Eds W.-Y.P. Wang, K.-F. Liu and Y. Tzeng (World Scientific, Singapore, 1989).
- [51] G.G. Ohlsen, Rep. Prog. Phys. **35**, 717 (1972);  
G.G. Ohlsen and P.W. Keaton, Jr, Nucl. Instr. Meth. **109**, 41 (1973).
- [52] D.V. Bugg and C. Wilkin, Phys. Lett. **B152**, 37 (1985).
- [53] T. Motobayashi *et al.*, Phys. Lett. **B233**, 69 (1989);  
S. Kox *et al.*, Phys. Lett. **B266**, 264 (1991) ;  
S. Kox *et al.*, To appear in Nucl. Phys. A (1993).
- [54] M. Garçon *et al.*, Nucl. Phys. **A458**, 287 (1986).
- [55] J. Carbonell, M. Barbaro and C. Wilkin, Nucl. Phys. **A529** (1991) 653.
- [56] E. Tomasi-Gustafsson *et al.*, LNS/Ph Report # 91-27 (1991), Saclay, unpublished.
- [57] LNS Proposal # 253, unpublished, (S. Kox : spokesperson).
- [58] CELEG, D. Joyce, CEBAF, March 1992.
- [59] V. Breton, Clermont-Ferrand Report and private communication.
- [60] G. Jones and J. van der Brand, Workshop...

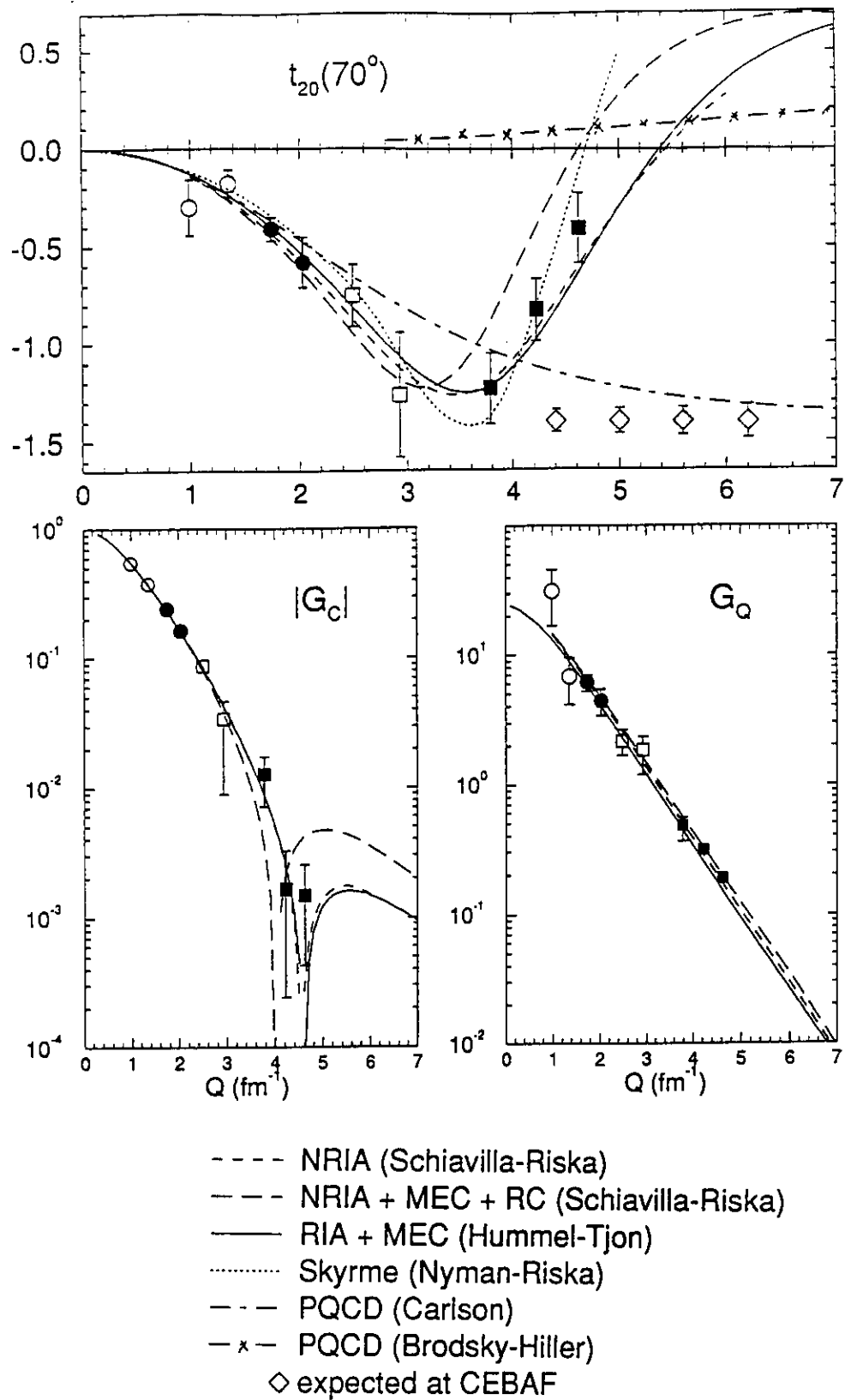


Figure 1 : Predictions of various theoretical models for  $t_{20}$ ,  $G_C$ ,  $G_Q$ , as a function of the momentum transfer to the deuteron. Experimental available data for  $t_{20}$  are displayed with their error bars (open circles [5,6], full circles [4], open squares [7], full squares [10]), as well as the range covered by this proposal (open diamonds), shown with the expected accuracy of the measurement.

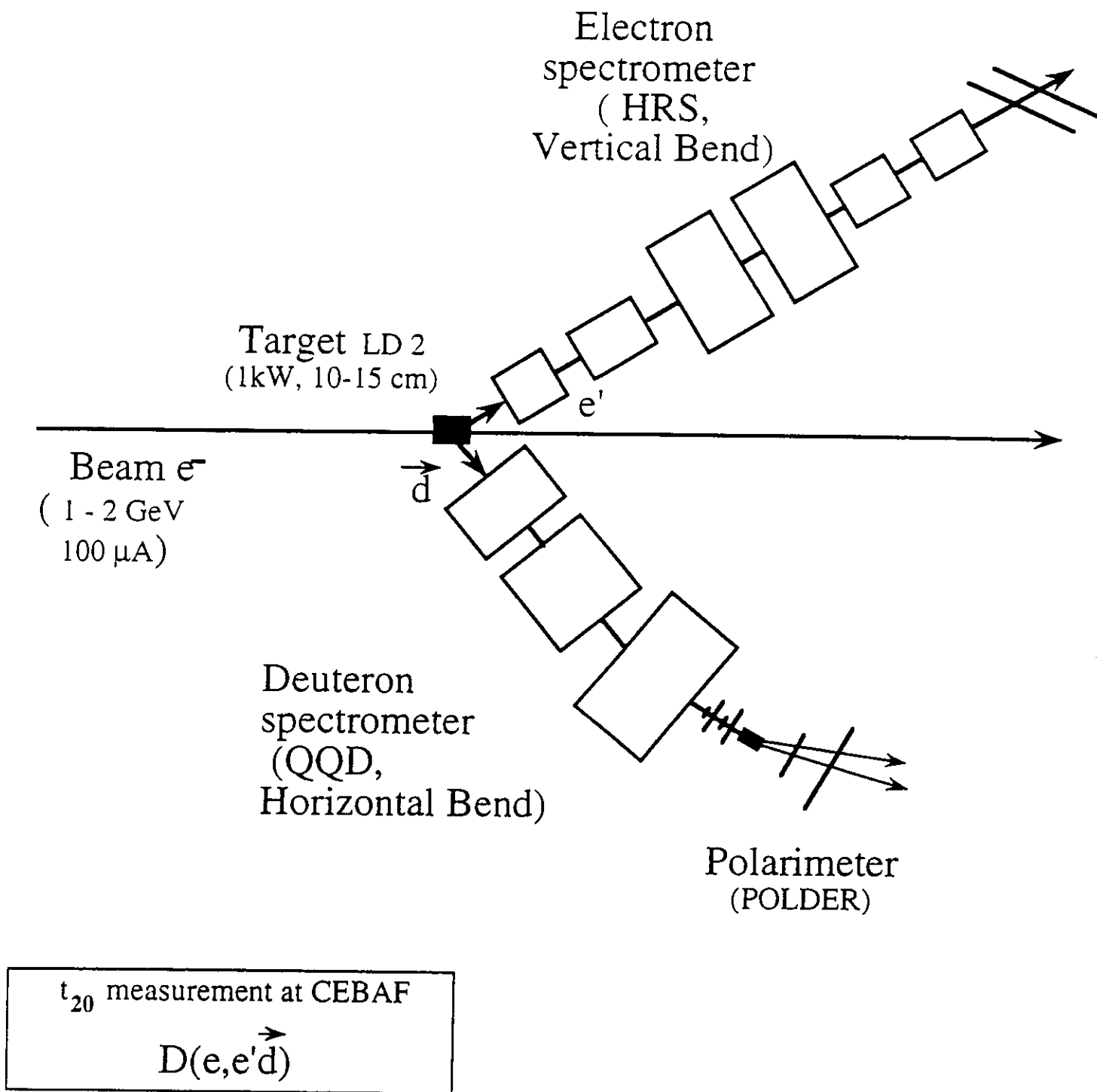


Figure 2 : Schematic lay-out of the  $t_{20}$  measurement at CEBAF (see text for details).

Kinematical factors for  $Q = 6.2 \text{ fm}^{-1}$

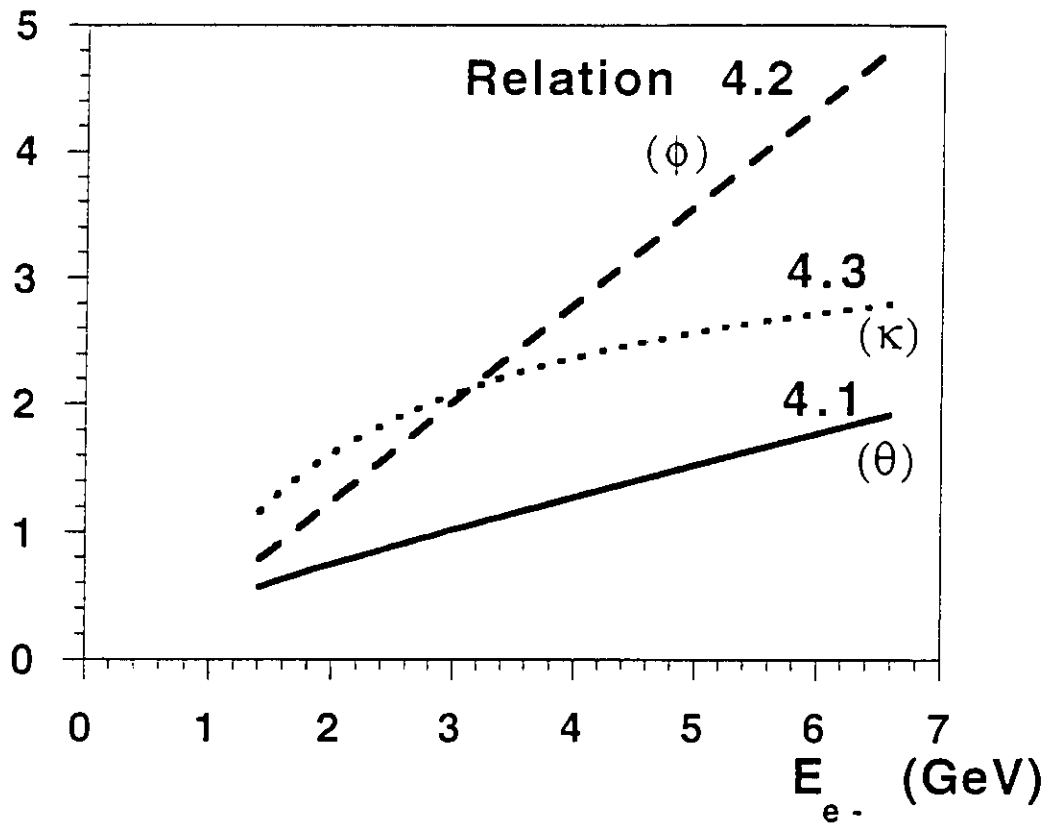


Figure 3 : Kinematical factors calculated for different beam energies. (see relations 4.1 to 4.3).

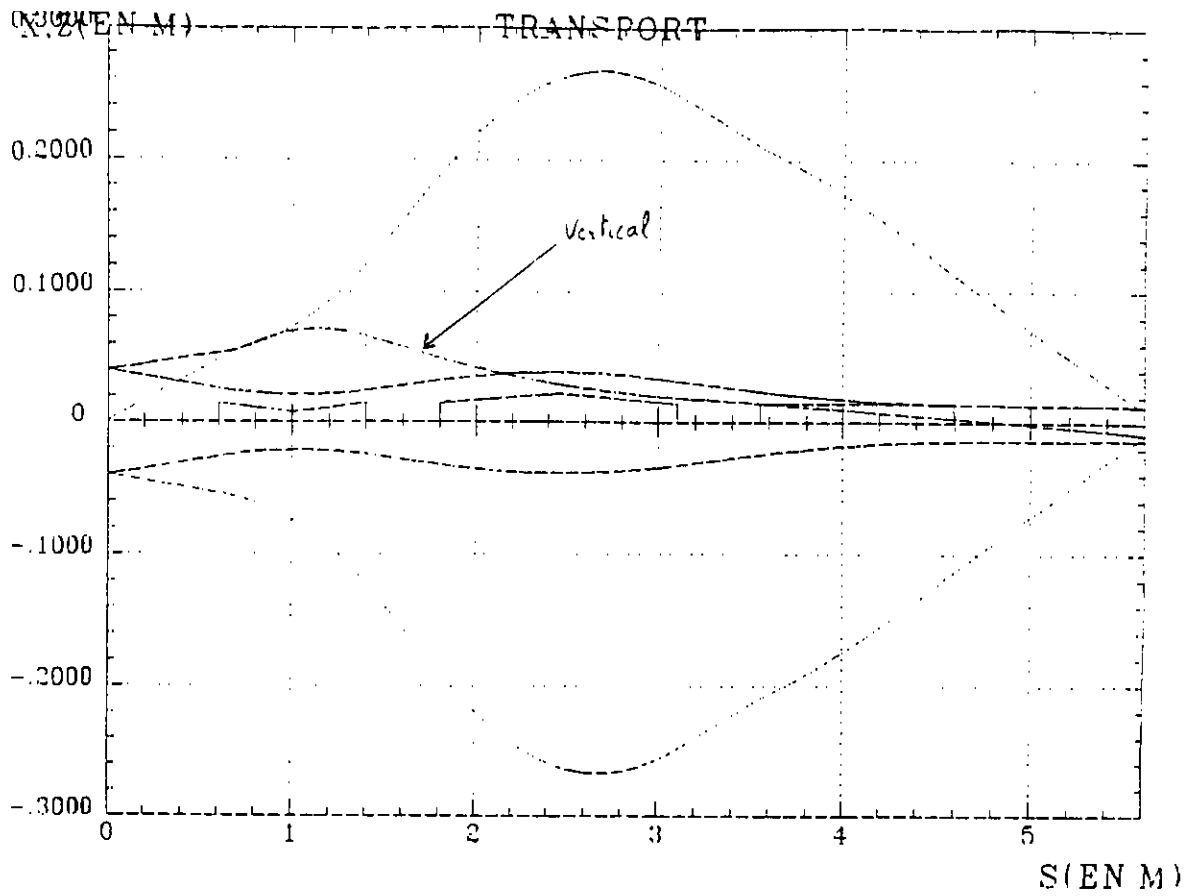


Figure 4 : Trajectories in the deuteron transport channel calculated for deuteron produced at  $\pm 4$ cm of the center of the primary  $LD_2$  target.

@ 5,596 ~

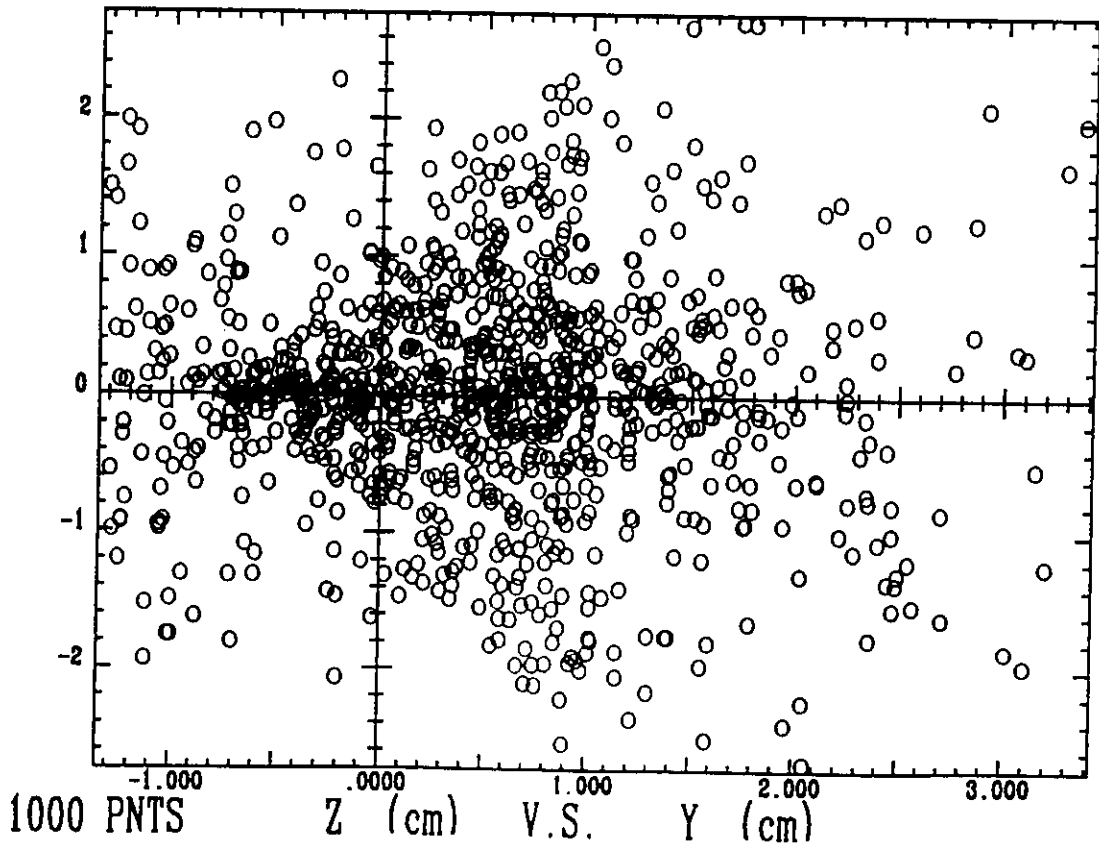
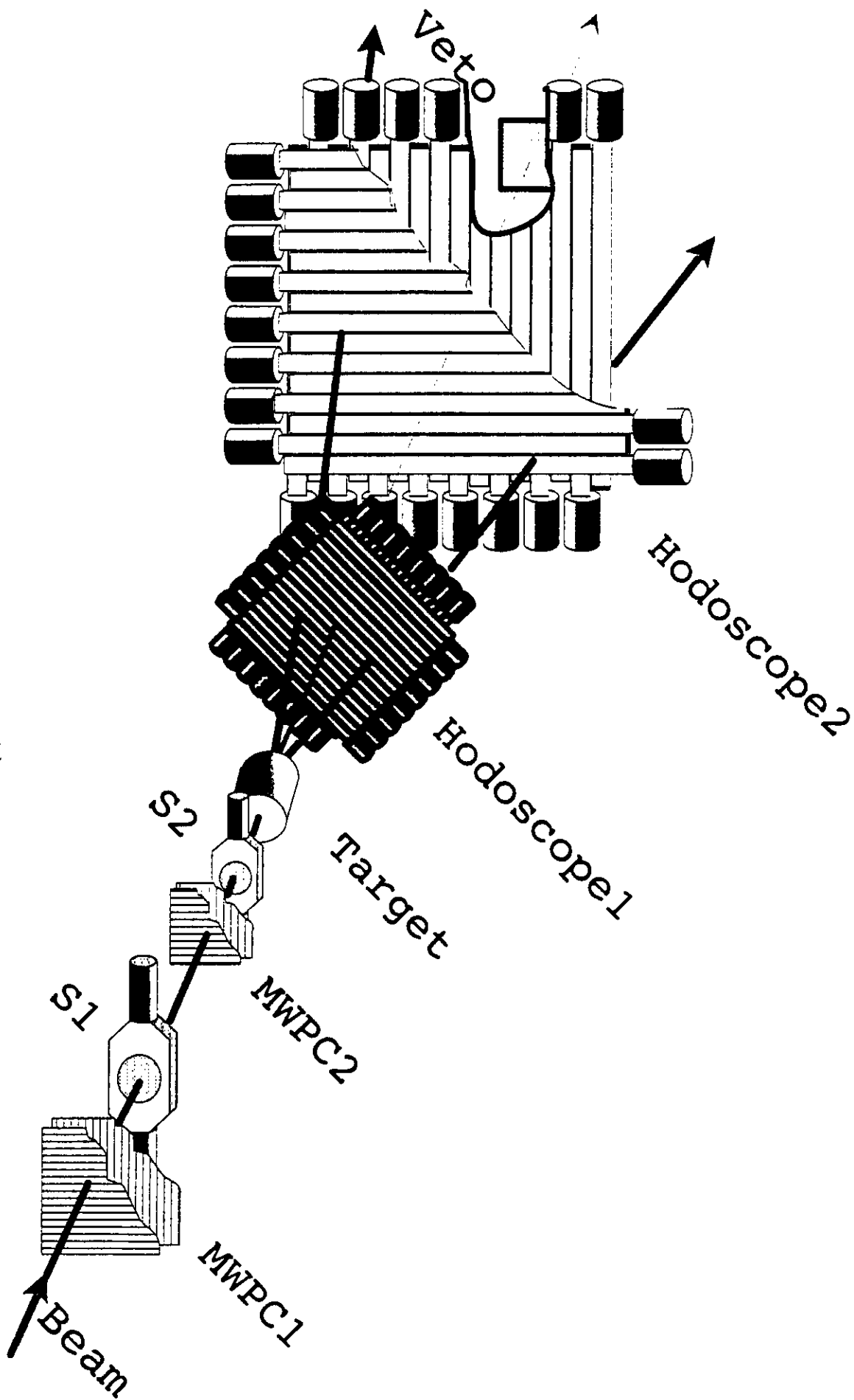


Figure 5 : Impacts of the deuterons on the polarimeter target after the transport channel

Figure 6 : Artist view of the *POLDER* polarimeter (see text for details).



## EXPERIMENT and SIMULATION

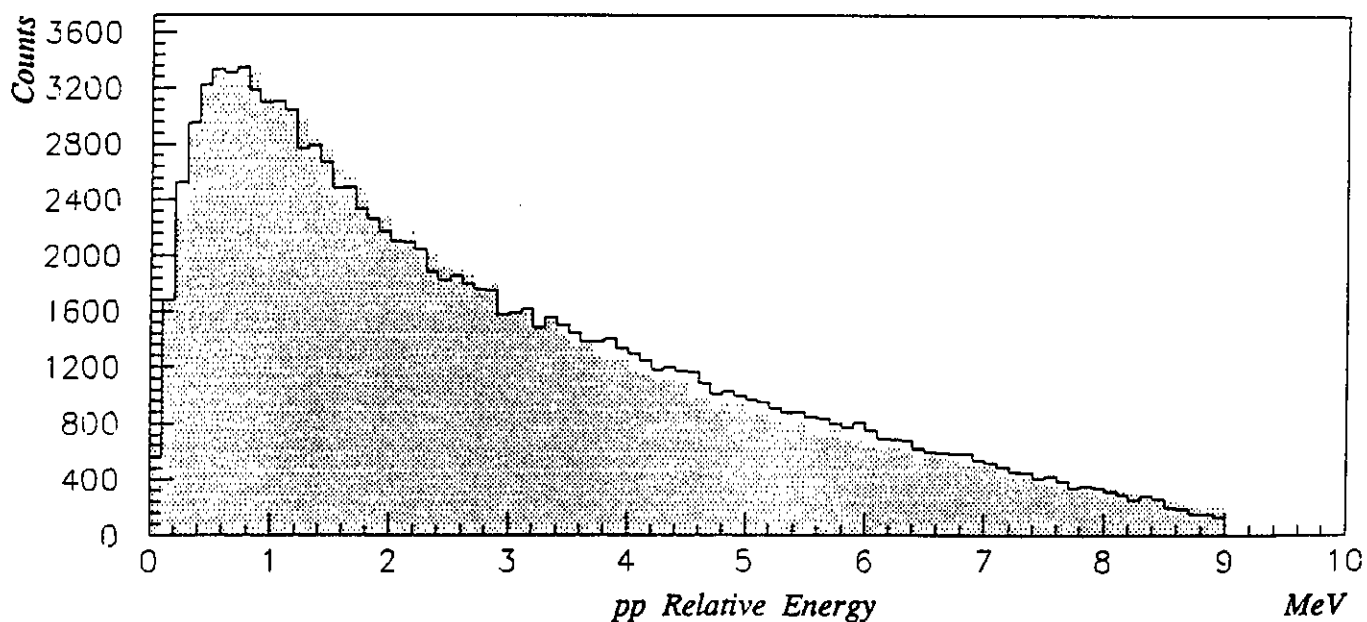
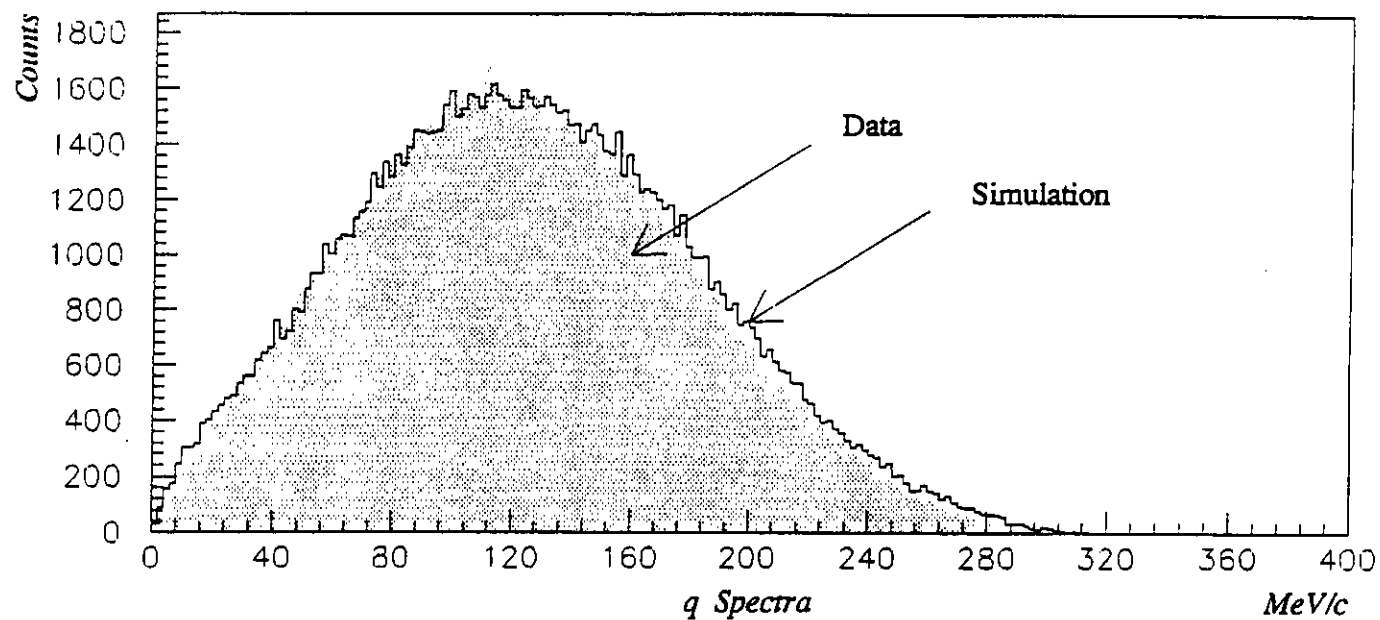


Figure 7 : Comparison of the experimental and simulated (see text)  $q$  and  $E_x$  spectra. Simulation inputs are the impulse approximation model which has been shown to describe well the  ${}^1\text{H}(\vec{d}, 2p)n$  reaction [57]. The agreement observed demonstrates the validity of data handling and rejection criteria.

## Integrated Efficiency of POLDER (Ex<5MeV)

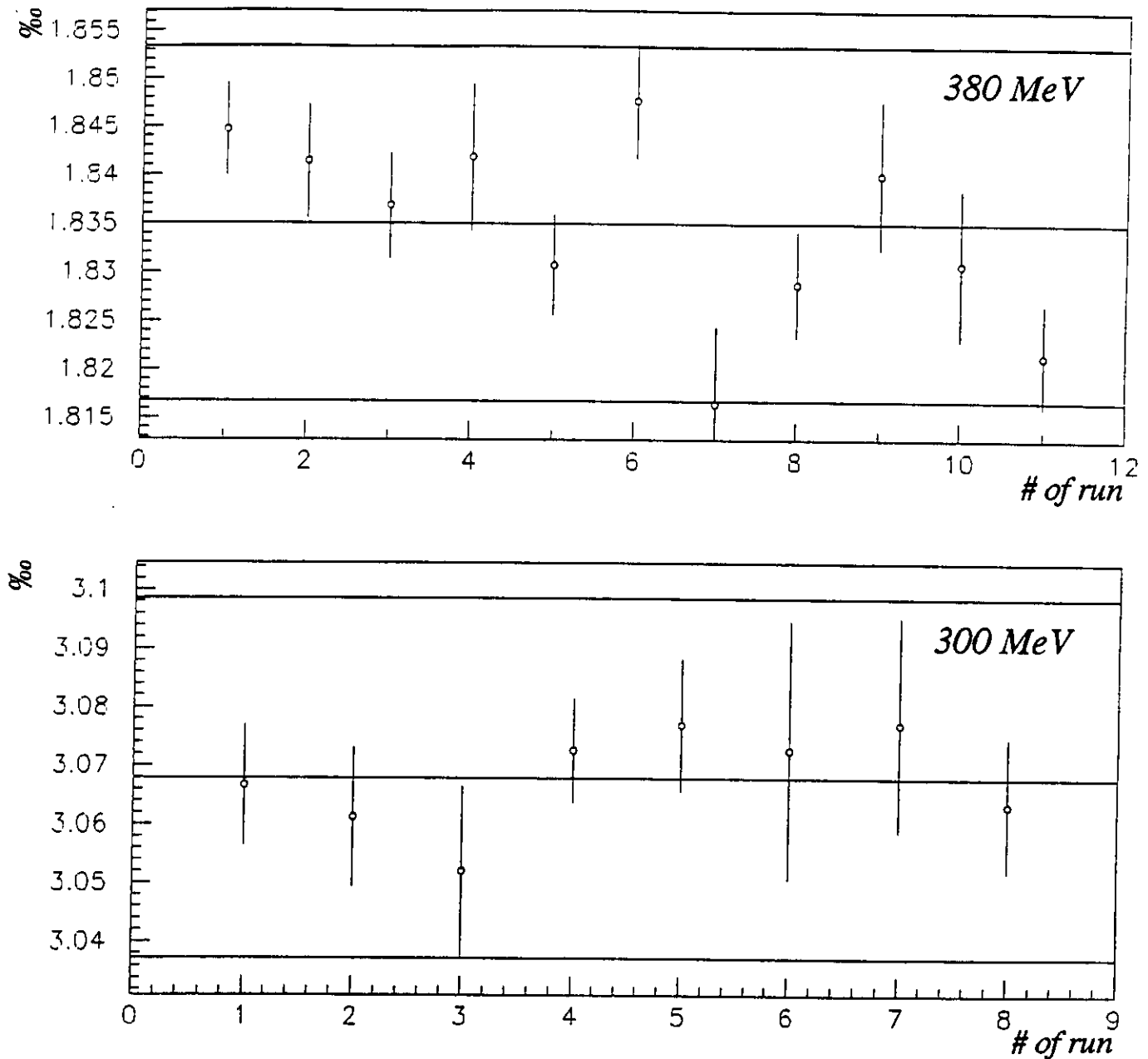


Figure 8 : Total detection efficiency of the *POLDER* set-up for the the  ${}^1\text{H}(\vec{d}, 2\text{p})\text{n}$  reaction in the excitation bin 0-5 MeV. The efficiency is shown for different runs of the calibration measurement at incident energies of 300 and 380 MeV and performed under very different experimental conditions. The mean value is drawn as solid straight lines as well as values at  $\pm 1\%$ .

# Ed = 380 MeV

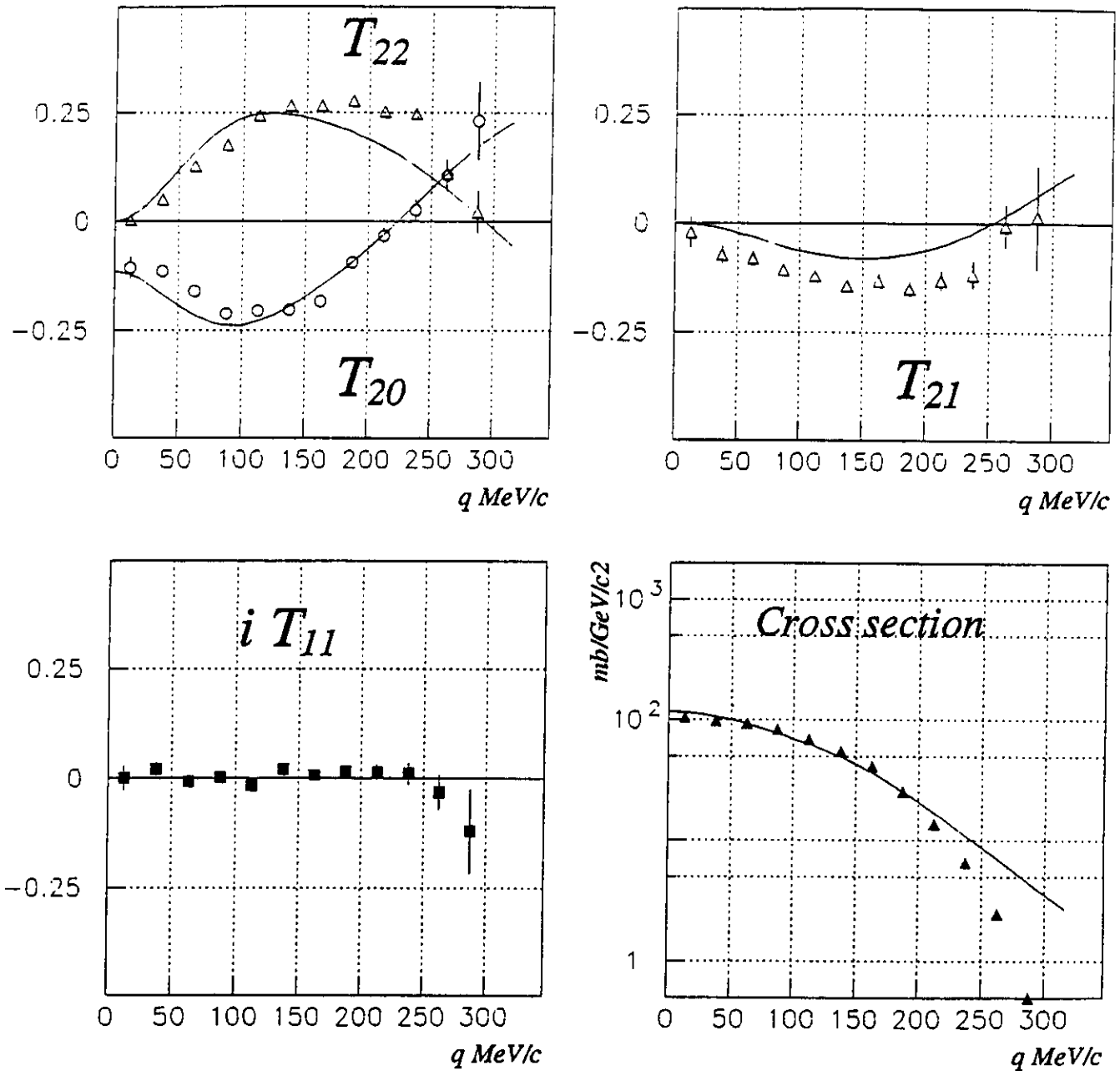


Figure 9 : Spherical analyzing powers and unpolarized cross section measured with the *POLDER* polarimeter for 380 MeV deuterons. The bin in excitation energy ( $E_x$ ) of the pp pair is 0-5 MeV. The solid curves are theoretical predictions of the impulse approximation model [57] for a 0-8 MeV bin in  $E_x$ . They can only be used as an eye-guide as data were not corrected for the detection efficiency and excitation energy resolution effects.

**Ed = 300 MeV**

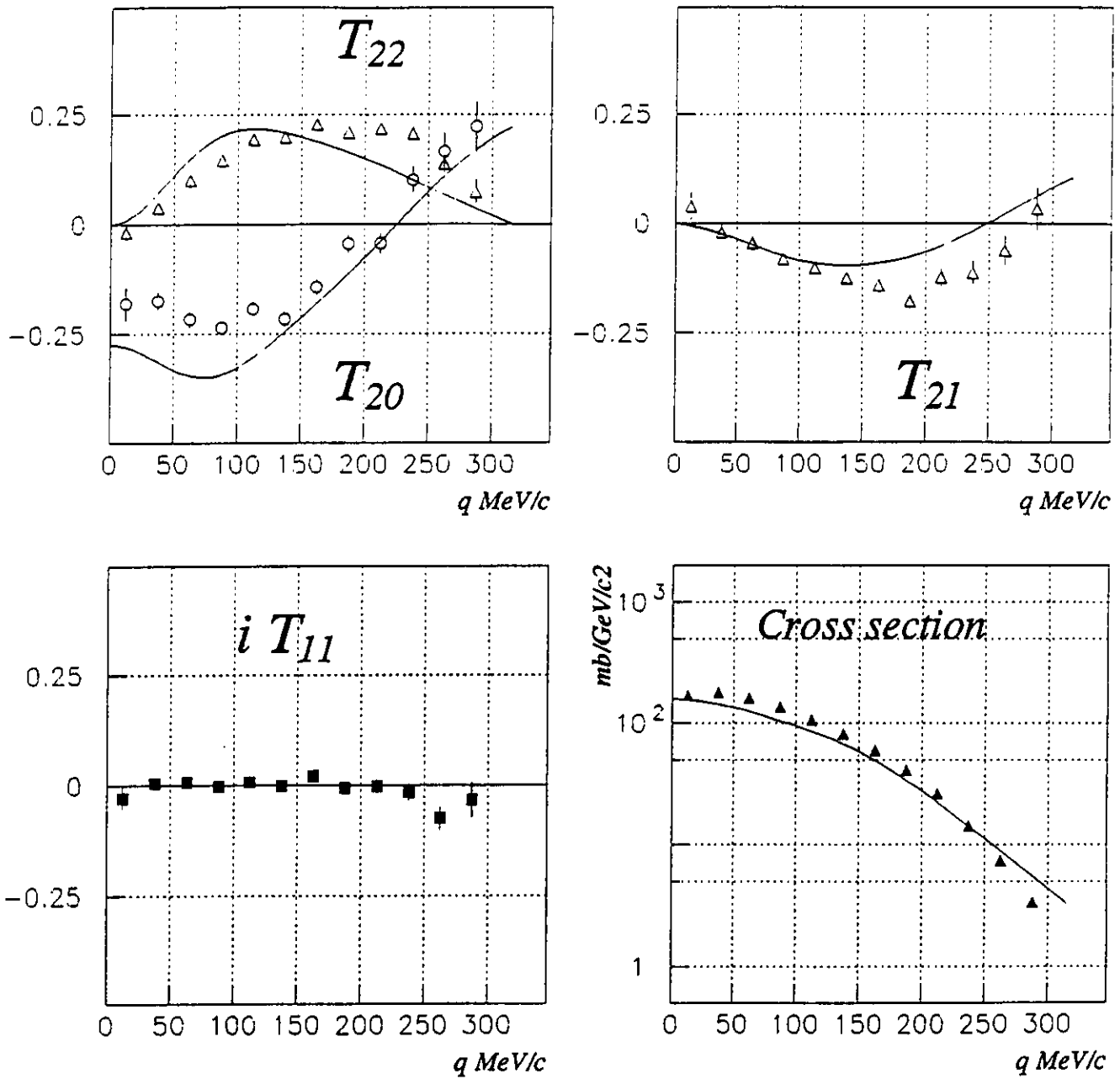


Figure 10 : Same as figure 9, but for 300 MeV deuterons.

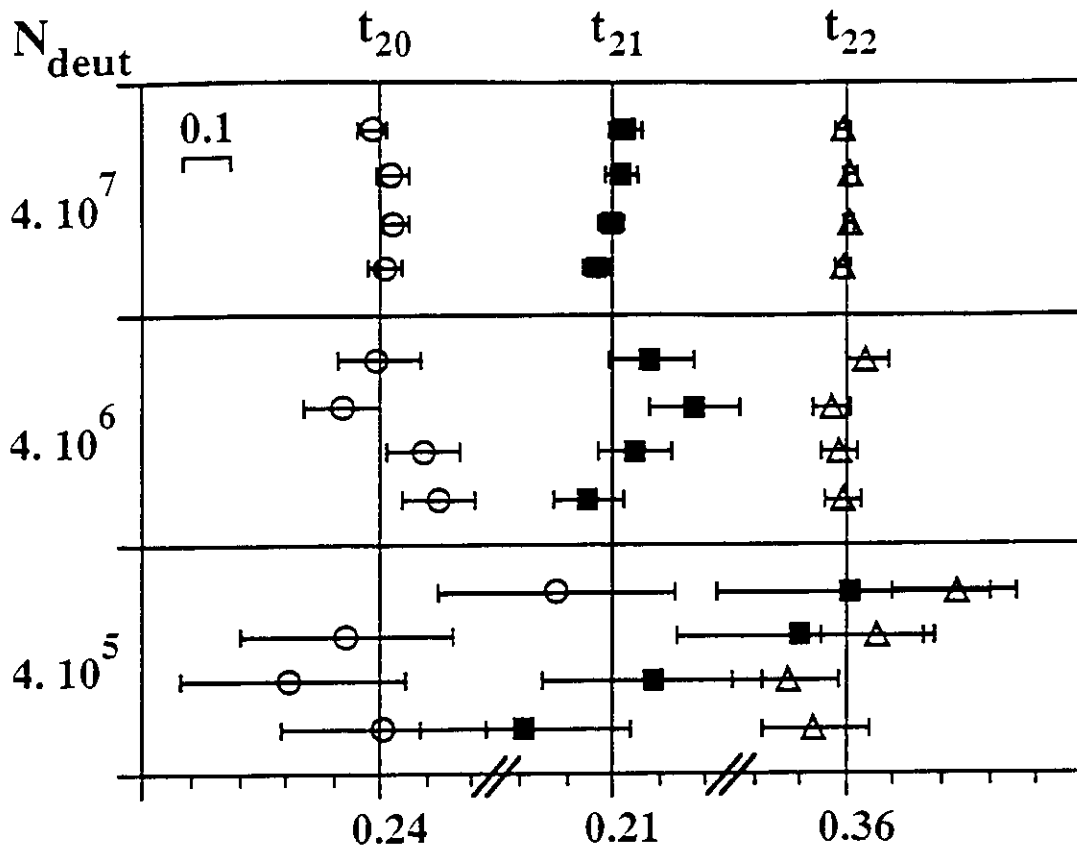


Figure 11 : Deuteron polarization measured by POLDER. The polarimeter has been calibrated using the whole set of data and a sample of data was analyzed in polarimeter mode. Values measured by the low energy polarimeter prior to the acceleration are indicated by a vertical line. This figure displays the results for 3 different numbers of incident deuterons on the polarimeter. (see text for the errors).

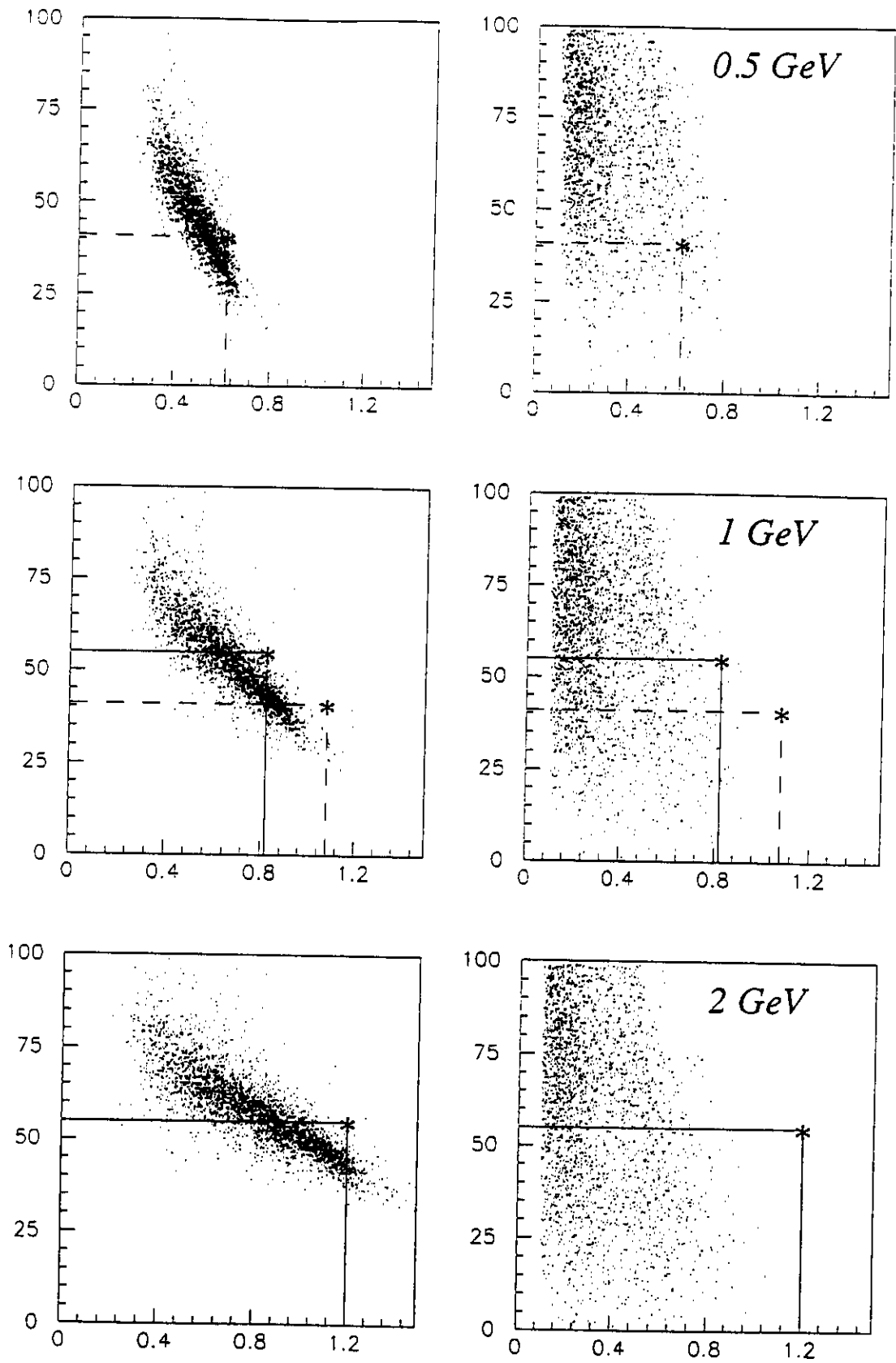


Figure 12 : Proton rates produced by quasi-elastic scattering (left part of the figure) and photo-disintegration of deuteron (right) processes. The events are plotted as a function of their angle (y axis) and momentum (x). Three different beam energies have been considered. Dotted lines show the experimental angle and momentum for the Bates experiment [10] whereas solid line shows those chosen in this proposal.

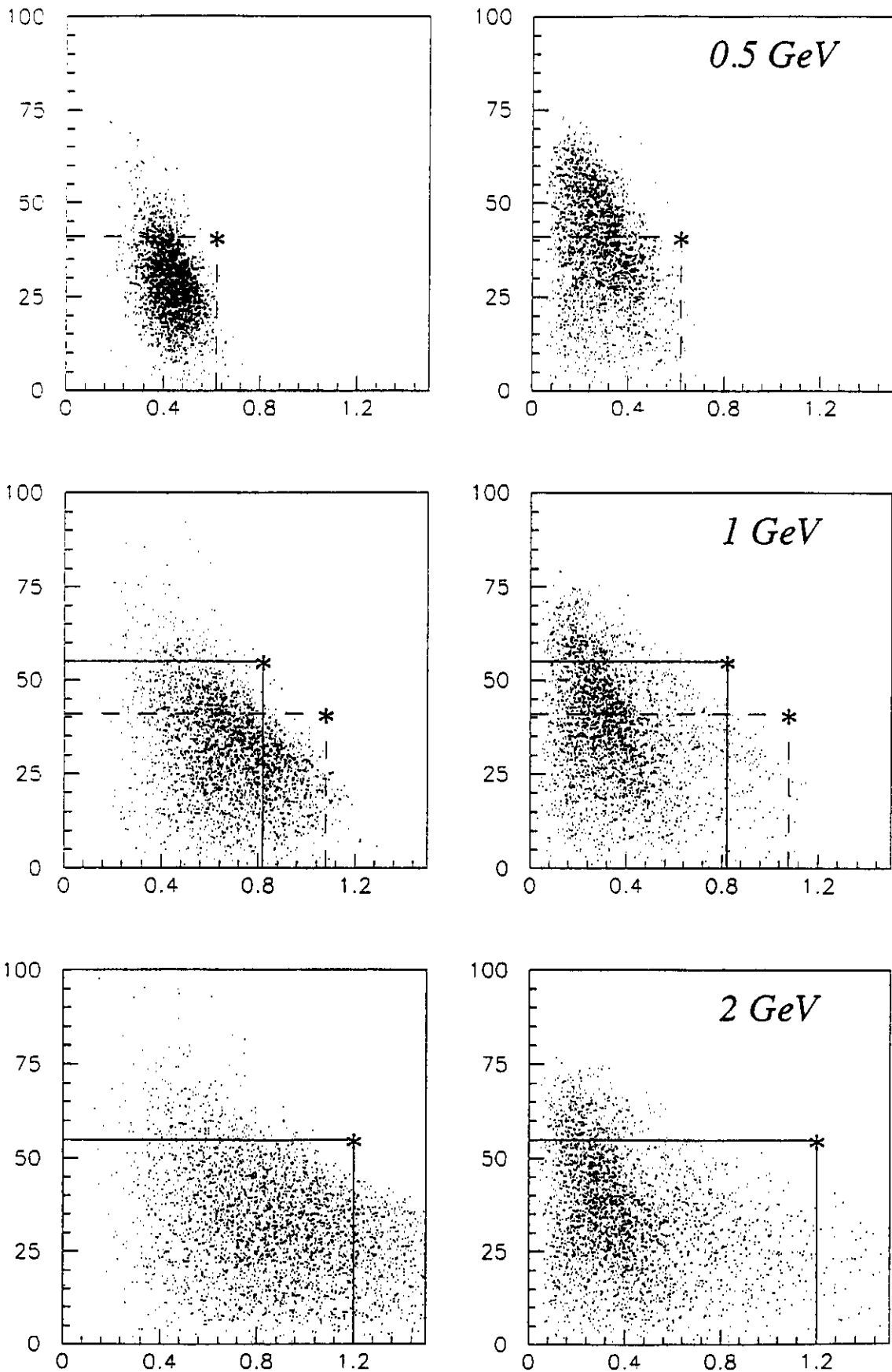


Figure 13 : Same as fig. 12 but for electro-(left) and photo-production (right) of  $\Delta$  and  $N^*$  resonances.